Chemical Science

ROYAL SOCIETY OF CHEMISTRY

PERSPECTIVE

View Article Online
View Journal | View Issue

Cite this: *Chem. Sci.*, 2025, **16**, 21152

All publication charges for this article have been paid for by the Royal Society of Chemistry

Received 14th August 2025
Accepted 21st October 2025

DOI: 10.1039/d5sc06220a

rsc.li/chemical-science

Multiplexed RNA imaging and *in situ* profiling in living cells

Lan Mi,†[a] Sima Khajouei†[a] and Mingxu You *[ab]

Single-cell *in situ* RNA profiling and multiplexed imaging have transformed our ability to uncover cellular heterogeneity by resolving distinct gene expression signatures. While established spatial transcriptomics methods – such as fluorescence *in situ* hybridization and *in situ* sequencing—have been widely used to map RNA profiles, they are inherently limited by the need for cell fixation and permeabilization, providing only static snapshots. In contrast, recent development of advanced fluorescent probes now enables multiplexed RNA imaging in living cells, offering a powerful way to monitor RNA localization, interaction, and concentration changes in real time. These innovations open new avenues for spatiotemporal *in situ* RNA profiling, making it possible to track RNA dynamics and unravel temporal relationships among multiple RNA species – longstanding challenges that remained out of reach with conventional approaches. This perspective highlights emerging advances in live-cell multiplexed RNA imaging, while also situating them alongside fixed-cell spatial transcriptomics methods, and discusses how these technologies can reshape our understanding of RNA biology and accelerate applications in disease mechanism studies, diagnostics, and therapeutic development.

1 Introduction

RNAs play essential roles in cells, notably as messengers in guiding protein synthesis (*e.g.*, mRNAs) or during transcription or epigenetic processes in regulating gene expression (*e.g.*, various non-coding RNAs).[1,2] These RNA functions are closely tied to their spatiotemporal dynamics and subcellular localization. For example, mRNAs often display tightly controlled spatiotemporal localization within dendrites, axons, and organelles such as mitochondria and endoplasmic reticulum (ER) to enable localized protein synthesis.[3] While long non-coding RNAs are more broadly distributed throughout the cell, where they exert regulatory functions across multiple stages of gene expression.[4,5] To study these spatially confined and dynamic processes, robust imaging techniques need to be developed to visualize and track RNA molecules within living systems.

However, most existing imaging approaches have traditionally focused on detecting only a single RNA species at a time,[6–9] which limits analytical throughput and increases the risk of false positives and false negatives in applications such as cell profiling, pathogen detection, and disease diagnostics. In reality, cellular processes are coordinated by networks of RNAs that act together rather than by individual transcripts. For instance, cancer is associated with the aberrant expression of multiple tumor-related genes, many of which can also show fluctuating expression in healthy cells. Cancer diagnosis relying on a single biomarker therefore often lacks sufficient specificity. Multiplexed gene detection offers a way to overcome this challenge. The multiplexing capability not only enhances the accuracy of early cancer diagnosis but also provides deeper insights into complex gene regulatory networks that drive health and disease.[10–12]

Multiplexed RNA imaging platform is such a system where multiple RNA species are detected and visualized within the same cell, ideally simultaneously with single-molecule precision. By leveraging strategies such as spectrally distinct fluorophores, iterative hybridization cycles, and/or combinatorial barcodes, multiplexed RNA imaging techniques can now enable the comprehensive mapping of gene expression patterns with high spatial resolution. On one hand, multiplexed RNA imaging in fixed cells or tissues has been dramatically advanced during the past years, especially with the development of multiplexed single-molecule fluorescence *in situ* hybridization (FISH) techniques, such as multiplexed error-robust FISH (MERFISH) and sequential FISH (seqFISH).[13–15] Quantitative detection of individual RNA transcripts with subcellular resolution can now be achieved, enabling transcriptome-wide detection with high spatial resolution.[16,17] In parallel to these imaging techniques, next-generation sequencing (NGS)-based spatial transcriptomics platforms are also gaining maturity. For instance, 10× Genomics Visium can capture RNAs on barcoded arrays,

[a]*Department of Chemistry, University of Massachusetts, Amherst, MA, 01003, USA. E-mail: mingxuyou@umass.edu*

[b]*Molecular and Cellular Biology Program, University of Massachusetts, Amherst, MA, 01003, USA*

† These authors contributed equally.

which are then sequenced and mapped back to their locations in the fixed tissues.[18] While in comparison to imaging-based *in situ* hybridization and *in situ* sequencing techniques, these NGS-based methods typically cannot offer high-resolution single-cell or subcellular level details regarding their RNA signatures.[19]

On the other hand, these fixed cell RNA imaging and profiling techniques hold several major restrictions. First of all, fixed-cell imaging or biochemical fractionation can only capture a single static time point in the cellular RNA lifecycle. These methods don't allow real-time tracking of RNA localization, movement, and interactions, offering limited dynamic or temporal information during real living processes. Meanwhile, the fixation procedure itself may induce artifacts by altering the localization and amount of target RNAs.[20,21]

In contrast, live-cell RNA imaging enables real-time analysis on how RNA behaviors correlate with other RNAs, proteins, or organelle dynamics. Cell selection and sorting can also be achieved based on the obtained dynamic gene expression profiles. Meanwhile, these live-cell tools can facilitate our understanding of how RNA transport, localization, translation, and decay will respond to RNA perturbation, cellular changes, or drug treatment. A growing number of live-cell multiplexed RNA imaging techniques have emerged recently, including synthetic oligonucleotide-based probes, bacteriophage-derived RNA labelling tags, CRISPR-dCas systems, fluorogenic RNA aptamers, and RNA-stabilized protein tags, as will be discussed in detail in the following sections. These approaches have begun to enable simultaneous observation of different RNA behaviors in living cells, adding a crucial temporal dimension to RNA studies and providing insights that are inaccessible through static analyses in fixed cells.

In this perspective, our goal is to provide an overview of available multiplexed RNA imaging technologies, with a particular emphasis on recent advances that enable dynamic RNA studies in living systems. We will trace the evolution from early single-target FISH methods to the development of highly multiplexed spatial transcriptomics approaches, and finally to the emerging platforms capable of visualizing multiple RNA species in real time within living cells. Our focus is to highlight how innovative analytical designs have driven these advances, discuss the current challenges of achieving multiplexing under physiological conditions, and explore how next-generation live-cell imaging strategies are poised to transform our ability to study gene expression dynamics, RNA localization, and cellular heterogeneity.

2 Advanced techniques for multiplexed RNA imaging and profiling in fixed cells and tissues

Our discussion starts with advanced RNA imaging and profiling technologies in fixed cells and tissues, which have allowed the detection of RNA localization and quantification at whole-transcriptome levels. The design principles of these techniques may also be potentially applied to inspire new multiplexed RNA imaging approaches for living systems. Here, we will classify these techniques into three main categories based on their detection mechanisms: *in situ* hybridization (ISH), *in situ* sequencing (ISS), and non-*in situ* next-generation sequencing (NGS).

2.1 *In situ* hybridization techniques

Fluorescence *in situ* hybridization (FISH) was first used for RNA detection in the early 1980s,[22] where fluorophore-conjugated DNA probes were designed for targeting actin mRNA in chicken muscle cells from tissue culture (Fig. 1a). In 1998, the emergence of single-molecule FISH (smFISH) really revolutionized RNA imaging by allowing for precise visualization and quantification of individual RNA molecules.[23] In 2002, simultaneous detection of over 10 cellular RNA transcripts was achieved by the Singer group *via* a combination of labelling probes with at least two distinct colors for each RNA target (Fig. 1b).[24] Such a spectral "barcoding" approach was further combined with spatially resolved order of labelling fluorophores in super-resolution microscopy to enable ~30 RNA species to be simultaneously analyzed in single yeast cells (Fig. 1c).[25]

Being powerful for studying single-cell RNA profiles, these early smFISH techniques were still limited in their multiplexing capability due to constraints in available fluorescence channels for simultaneous imaging. An important innovation that significantly increased the scalability of FISH is the incorporation of a sequential imaging and stripping approach, which leads to the development of highly multiplexed approaches: MERFISH and seqFISH.[13–15] In the original seqFISH technique developed by the Cai group, 12 unique RNA transcripts in budding yeast were identified by using four-color DNA probes in two rounds of imaging: each RNA was initially imaged with one of the four fluorescent probes, and then the probes were removed by DNA digestion, followed by re-staining with a second round of four-color probes. Theoretically, this two-round approach can enable discrimination of 16 individual RNAs ($4^2 = 16$).[14]

The MERFISH approach, first introduced by the Zhuang group in 2015, has dramatically improved the throughput of RNA imaging.[13] A major difference between seqFISH and MERFISH lies in their barcoding strategies to differentiate RNA species. SeqFISH (and similarly osmFISH[26]) uses a dye-labeled DNA strand to target RNA species directly, while MERFISH separates the targeting strands from the readout strands by assigning each RNA molecule to a unique N-bit binary barcode during N rounds of readout (Fig. 1d). In each round of imaging, a readout strand is added to reveal whether a specific RNA emits fluorescence (bit 1) or remains undetected (bit 0). After imaging, the dye is photobleached, and a new readout probe is then introduced. With a typical N (~14–16) rounds of such repeated procedure, a maximum of 2^N–1 RNAs (*i.e.*, ~16 000–65 000) can be detected.

A key feature of MERFISH is the introducing of a Hamming distance of 2 or 4 that allows error-robust encoding, where ≥2 or 4 reads must be incorrect to avoid being assigned as a correct target RNA. As the same dye-labeled readout strand was used to

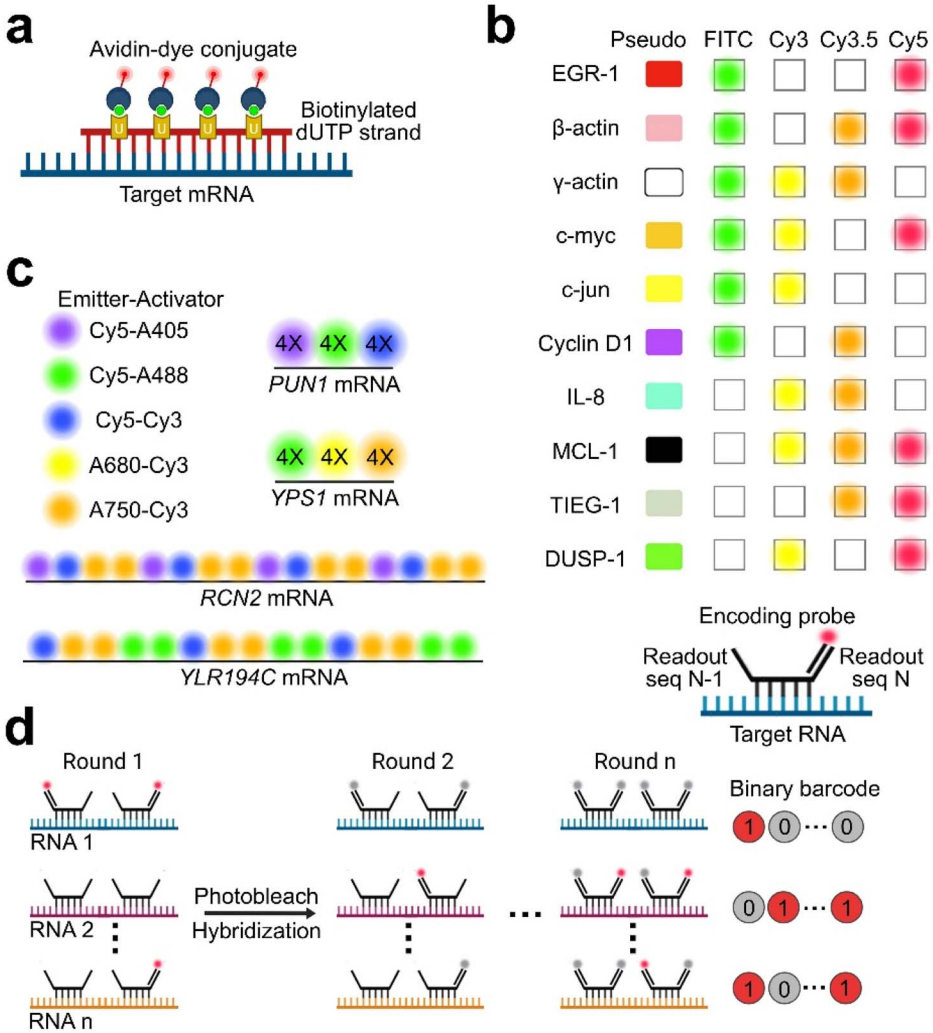

Fig. 1 (a) A sample fluorophore-conjugated DNA probe designed for recognizing target messenger RNA. (b) Simultaneous imaging of 10 cellular RNAs can be achieved *via* the use of color groups. At least two colors were used for each RNA transcript to reduce the chance of single-color false positive signals. Reproduced from ref. 24 with permission from the American Association for the Advancement of Science, copyright 2002. (c) A spectral barcoding method that applies super-resolution imaging techniques to detect ~30 RNA targets. Shown are some sample illustrations of colors used for barcoding four mRNA species. (d) Schematic of MERFISH, a multiplexed smFISH method using combinatorial labelling and error-robust encoding. Encoding probes are designed to contain RNA-binding regions flanked by two readout sequences. A specific combination of four readout sequences encodes each RNA species. Sequential hybridization rounds with fluorescent readout probes detect these sequences, with photobleaching between rounds.

simultaneously detect different RNA targets in an imaging round, the cost of probe synthesis and time required for hybridization can be dramatically reduced. MERFISH initially can enable the multiplexed analysis of approximately 100–1000 RNA species,[13] which offers a reliable method that paves the way for further spatial transcriptomic studies in capturing whole-transcriptome information at distinct cellular states. By integrating MERFISH with expansion microscopy, ~10-fold higher total density of RNAs have been profiled in a single experiment.[27]

In another critical study, seqFISH+ was developed to allow transcriptome-wide imaging by enabling the detection of ~10 000 genes in single cultured cells as well as in mouse brain tissues.[28] By using a sparse labelling strategy to lower the RNA density, only a subset of targets was hybridized and detected in each round of seqFISH+. Meanwhile, super-resolution microscopy in three different fluorescent channels (*i.e.*, a ~60 bit binary barcode) was employed to spatially resolve these RNA transcripts and increase throughput of the whole imaging process.

As the throughput of these *in situ* hybridization techniques has been dramatically increased, more efforts have been spent on enhancing their other analytical properties, including the detection accuracy, sensitivity, and signal-to-noise ratio. Split-FISH is such an imaging method for reducing background noise and false positives in non-cleared tissues.[29] This strategy uses a split-probe design, where two adjacent probes hybridize near each other on the target RNA. A bridge strand is then

added that can only generate signals upon cooperative binding with two nearby split probes. Split-FISH have been successfully used to quantify the spatial distribution and abundance of 317 genes at single-cell resolution in complex tissue samples.[29]

RNAscope is another widely adopted *in situ* hybridization platform that uses adjacent pairs of "double Z" probes to precisely target RNA molecules.[30] This arrangement forms a distinct binding site that initiates a multi-stage signal amplification process, enhancing both sensitivity and specificity of RNA detection by reducing background noise. Such probe design is also suitable for tissue samples and compatible with automated systems. As another example of smFISH techniques with increased signal-to-noise ratio, DART-FISH employs padlock probes along with rolling circle amplification (RCA) and a combinatorial barcoding strategy to detect hundreds to thousands of genes within tissue sections.[31] By incorporating enzyme-free isothermal decoding steps and reducing the number of imaging cycles, DART-FISH facilitates efficient and scalable spatial transcriptomic analysis in complex biological tissues within a more reasonable timeframe, *e.g.*, 121 genes can be successfully identified across a large (~30 mm) human tissue sample in <10 hours.

It is worth noting that such *in situ* hybridization-based multiplexed RNA imaging techniques have been successfully commercialized for automated single-cell resolution spatial transcriptomic profiling in tissue samples, such as that shown in Vizgen MERSCOPE and NanoString CosMx.[32–35] These smFISH-based techniques have significantly advanced our capability of high-resolution subcellular RNA profiling at the entire transcriptome-level.

2.2 *In situ* sequencing methods

In situ sequencing (ISS) technologies represent another significant evolution in spatial transcriptomics. Unlike smFISH-based methods that rely on the hybridization of fluorescent probes to pre-selected RNA targets, ISS offers both targeted and untargeted approaches to sequence RNA transcripts directly inside cells or tissues. ISS can enable nucleotide-resolution transcript identification with spatial context, expanding the scope and granularity of cellular RNA profiling.

In targeted ISS that was first demonstrated by the Nilsson group in 2013, RNAs of interest were first *in situ* reverse transcribed into complementary DNAs (cDNAs), followed by RCA to produce repeated DNA copies as robust localized amplicons within the tissues and cells (Fig. 2a).[36] These amplified sequences were then decoded through a series of sequencing-by-ligation steps, during which one of four-color fluorescently labeled 9-mer random-sequence probes with one fixed A/C/G/T at a specific position was *in situ* ligated to an anchor primer. Each imaging cycle captures the identity of nucleotide at this position to distinguish different RNA targets. It is worth mentioning that the original sequencing-by-ligation chemistry exhibits quite low efficiency (~20–30%). Even by replacing with a hybridization-based ISS assay,[37] the detection efficiency and throughput of such targeted ISS techniques remain a major technical concern.

To further enhance the resolution and robustness of ISS, STARmap (spatially resolved transcript amplicon readout mapping)[38] and BOLORAMIS (barcoded oligonucleotides ligated on RNA amplified for multiplexed and parallel *in situ* analyses)[39] were developed by the Deisseroth group and Church group, respectively. STARmap introduced a two-component logic padlock probe system to reduce non-specific hybridization to cellular RNAs and inserted a five-base barcode ($4^5 = 1024$ possibility) for identifying particular RNA targets (Fig. 2b). Acrylic acid-modified DNA probes were used to copolymerize with acrylamide and embed into hydrogel for optical clearing. Meanwhile, an error-robust *in situ* sequencing-by-ligation chemistry called SEDAL was implemented to read the five-base barcode for multiplexed RNA localization. In each cycle of SEDAL, an increasing length of 5′-phosphorylated reading strand was mixed with fluorophore-labeled decoding strands. Only when the dinucleotides at the 3′-end of the decoding strand are fully complementary to the barcode sequence next to the reading position, a ligation occurred to give out detectable imaging signals. Afterwards, formamide was added to strip the probes and prepare for the next cycle. With all these advances, STARmap can achieve reliable detection of over 1000 genes in intact brain tissue, at an error rate of ~1.8%.

SEDAL-based *in situ* sequencing has also been used in another TEMPOmap technique that can interestingly map dynamic RNA synthesis, movement, and degradation events with subcellular precision.[40] By pulse-chase metabolic labelling nascent mRNAs with 5-ethynyl uridine, RNAs of interest can be selectively amplified and *in situ* imaged with temporal information (Table 1).

Another major advancement in ISS was the achievement of untargeted *in situ* sequencing. Unlike targeted ISS, methods like fluorescent *in situ* sequencing (FISSEQ)[41,42] uses adapter-fused random hexamers as primers to convert cellular RNAs into cDNAs without selecting particular genes. These cDNAs were circularized using enzymes like CircLigase II and amplified *in situ via* RCA. Subsequent ISS was then achieved *via* sequencing by oligonucleotide ligation and detection, commonly known as the "SOLiD" technology, yields genome–aligned reads. More specifically, a sequencing primer that is complementary to the adapter was ligated to dinucleotide-specific 8-mer fluorescent probe for imaging. Afterwards, the fluorophore and last three bases of the probe were cleaved to allow for additional ligation cycles to interrogate other dinucleotide pairs. While enabling unbiased transcriptome-wide profiling, FISSEQ faces several technical challenges, including inefficient RNA-to-cDNA conversion, optical crowding due to high transcript density, and the predominance of abundant RNAs like rRNA. As a result, a low detection efficiency (<0.2%) was often observed in FISSEQ.[19]

To address these issues, expansion sequencing (ExSeq) that integrates FISSEQ with expansion microscopy was developed by the Boyden group.[43] After anchoring RNAs to a hydrogel-based system, ExSeq physically expanded tissue samples to improve molecular resolution and reduce crowding, thereby enhancing both spatial clarity and gene detection in FISSEQ. Without requiring target amplification, the Wu group introduced

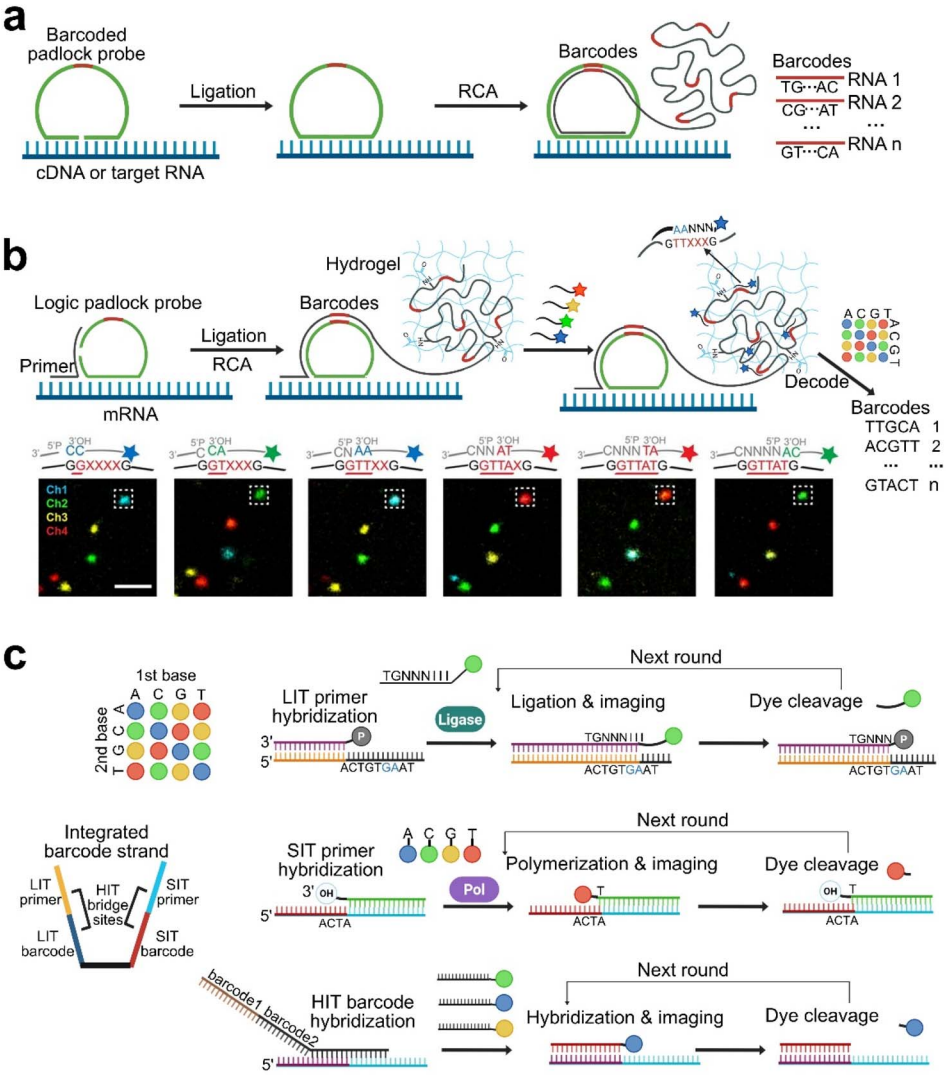

Fig. 2 (a) Schematic illustration of an *in situ* sequencing method where RNA transcripts or its corresponding cDNA is used to guide the self-ligation of barcoded padlock probes. Repeated DNA copies are then produced enzymatically *via* rolling circle amplification (RCA) with increased number of localized barcodes. (b) Overview of a STARmap technique where a primer is used to guide the ligation of logic padlock probe. RCA enzymatically replicated amplicons are then embedded in a hydrogel, *in situ* sequenced *via* a SEDAL sequencing-by-ligation approach *via* reading a five-base barcode to identify the particular RNA target. In each cycle of SEDAL., a 5′-phosphorylated reading strand is combined with fluorophore-labeled decoding strands. Ligation and signal detection occurs only when the decoding strand's 3′ dinucleotide perfectly matches the barcode sequence at the reading position. Sample images were reproduced from ref. 38 with permission from the American Association for the Advancement of Science, copyright 2018. Scale bar, 2 μm. (c) Overview of the barcode strand design and *in situ* sequencing methods used in an OligoFISSEQ technique. Top: sequencing-by-ligation approach *via* ligation of a phosphorylated primer to an 8-mer with fluorophore-coded dinucleotides. Middle: sequencing-by-synthesis approach that fluorophore-labeled nucleotides were used to identify barcode nucleotides. Bottom: sequencing-by-hybridization method that bridge oligos recruit barcode-specific probes, enabling full sequence determination in eight hybridization rounds.

OligoFISSEQ by integrating barcode strands of non-genomic sequences respectively with three ISS strategies, sequencing-by-ligation, sequencing-by-synthesis, and sequencing-by-hybridization (Fig. 2c).[44] OligoFISSEQ can also be used together with single-molecule localization microscopy, such as OligoSTORM[45] for super-resolved RNA detection.

Despite these improvements, the low detection efficiency of current sequencing chemistry and molecular crowding remain critical limiting factors for these untargeted ISS techniques. In contrast, targeted ISS approaches benefit from a more manageable transcript density, as the whole transcriptome can be divided into subsets of ~1000–2000 genes,[38] where each subset is imaged sequentially using short multi-color barcodes. Although such a division approach may increase the total imaging time, it avoids long barcodes to maintain a high detection efficiency. Targeted ISS approaches can be preferred for their nice balance of high accuracy, scalability, and efficiency.[19]

New *in situ* sequencing chemistry is highly desired to further improve the detection efficiency and accuracy of both targeted

Table 1 Techniques for multiplexed RNA imaging and profiling in fixed cells and tissues

Technique	Multiplexing	Resolution	Principle	Advantages	Limitations	Ref.
Barcoded smFISH	Up to ~30 RNAs	Single molecule	RNA labelling with distinct colors and spatial order	Quantitative simultaneous RNA imaging with high spatial precision	Limited number of fluorescence channels for multiplex imaging	24 and 25
MERFISH	Whole-transcriptome-scale	Single molecule	Sequential smFISH with combinatorial error-robust encoding	Quantitative error-robust full-transcriptome imaging	Long-time, repeated photobleaching cycles, photodamage potential	13 and 27
seqFISH(+)	Whole-transcriptome-scale	Single molecule	Sequential hybridization & imaging cycles	Quantitative full-transcriptome imaging with error correction	Long-time repeated cycles, many probes, potential photodamage	14 and 28
Split-FISH	>300 genes	Single molecule	Two probes hybridize adjacent regions in target RNA to increase specificity	Reduced background noise and false positives	Requires many probes, moderate multiplexing ability	29
DART-FISH	Up to ~300 genes	Single molecule	Barcoded RCA probes and *in situ* decoding	Increased signal-to-noise ratio, relatively fast	Tissue processing requires optimization, moderate multiplexing ability	31
STARmap	>1000 genes	Subcellular	Logic padlock-RCA probes with SEDAL *in situ* sequencing-by-ligation	Relatively error-robust, possibility to study 3D tissue samples	Sample preparation may affect RNA preservation, difficult in precise whole-transcriptome analysis	38
TEMPOmap	~1000 genes	Subcellular	Pulse-chase metabolic labelling with SEDAL *in situ* sequencing-by-ligation	Map both spatial distribution and temporal dynamics of RNA	Variant metabolic labelling efficiency. Difficult in precise whole-transcriptome analysis	40
FISSEQ	Whole-transcriptome-scale	Subcellular	Random primed *in situ* SOLiD sequencing	Unbiased transcriptome-wide profiling, possibility to conduct *de novo* analysis	Optical crowding and relatively low detection efficiency	41 and 42
ExSeq	>1000 genes	Subcellular	Expansion microscopy with targeted or untargeted *in situ* sequencing	Targeted or unbiased *de novo* RNA analysis with improved resolution	Long-time, many reagents, technically demanding	43
Visium	Whole-transcriptome-scale	~50 μm or ~20 μm (Ex-ST)	Barcoded slide spots capture RNA for NGS-based analysis	Widely adopted, easy to use	Limited resolution, potential multi-cell mixed transcriptomic signals	18 and 47
Slide-seq(V2)	Whole-transcriptome-scale	~10 μm	DNA-barcoded bead array for RNA capture and NGS-based analysis	Relatively high spatial resolution with single-cell-level resolution	Relatively low RNA capture efficiency, hard for low-abundance RNA detection	48 and 49
Seq-scope	Whole-transcriptome-scale	~0.6 μm	Illumina flow cell-based spatially barcoded arrays and NGS-based analysis	Subcellular resolution whole-transcriptome analysis	Relatively small capturing and detection area	50
Stereo-seq	Whole-transcriptome-scale	~0.5 μm	DNA nanoball-barcoded chips and NGS-based analysis	Subcellular resolution whole -transcriptome analysis with large field of view	Data complexity	51

and untargeted ISS techniques. Chemical strategies to selectively deplete highly abundant transcripts (*e.g.*, housekeeping RNAs) can also be helpful. Moreover, emerging computational tools are capable of inferring genome-wide gene expression from a targeted set. By integrating spatial data with single-cell RNA-sequencing profiles,[46] such hybrid strategies may offer a promising path forward in resolving transcriptomic heterogeneity across diverse tissue landscapes.

2.3 Non-*in situ* next-generation sequencing methods

Another frontier in spatial transcriptomics involves the integration of NGS technologies with spatial barcoding to achieve high-throughput RNA profiling. In these methods, RNA transcripts are often captured on spatially barcoded surfaces, after reverse transcription of RNA into cDNA, NGS is then performed to identify transcript sequences. The spatial origin of these transcripts can be inferred through pre-assigned barcodes and computational reconstruction. Unlike ISS or ISH techniques, which preserve cellular morphology, NGS-based methods require physical extraction of RNA from cells. We will only illustrate the working principles and chemistry of some representative NGS systems, with a goal to inspire future techniques for RNA profiling in living cells.

One pioneering approach in array-based spatial transcriptomics was introduced by Ståhl *et al.* in 2016,[18] which paved the foundation for the commercialized 10× Genomics Visium platform. In such a platform, tissue sections are placed on a microarray containing ~1000–5000 capture spots arranged within a ~6.5 × 6.5 mm^2 area (Fig. 3a). Each spot contains millions of fixed oligonucleotide probes composed of an Illumina sequencing primer, a spatial barcode, a unique molecular identifier, and a poly(dT) sequence for hybridization to polyadenylated mRNAs. Transcriptome-wide spatial information can be provided in these conventional array-based spatial transcriptomics, while a key limitation is its inability to achieve single-cell resolution detection as each ~50–100 μm in diameter spot may encompass multiple cells, leading to mixed transcriptomic signals.[18]

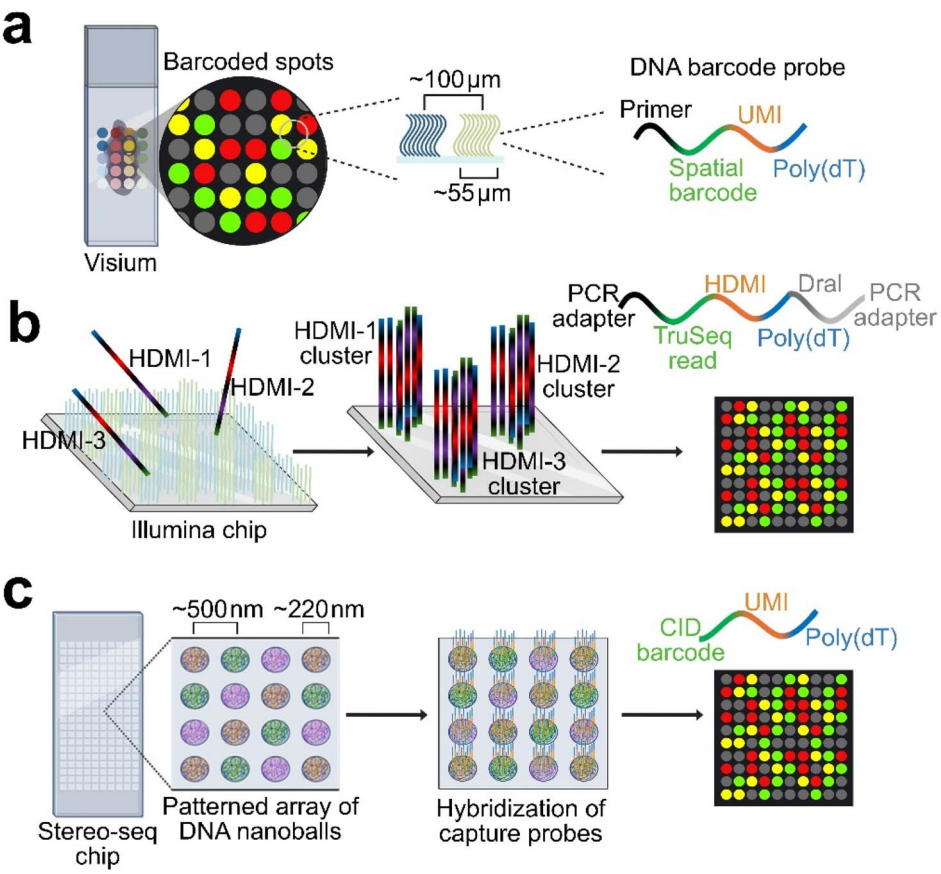

Fig. 3 (a) Schematic illustration of Visium technique. Each capture spot is embedded with millions of oligonucleotide probes engineered with a spatial barcode, a unique molecular identifier (UMI), an Illumina sequencing primer site, and a poly(dT) tail for selective mRNA binding. Following tissue permeabilization, polyadenylated mRNAs hybridize to these probes, enabling spatially indexed cDNA to be synthesized by reverse transcription and traced back to its original position within the tissue. (b) Overview of Seq-Scope spatial transcriptomics. The method creates clusters of oligonucleotides with high-definition map coordinate identifier (HDMI) on a flow cell surface. The structure of the HDMI-oligo library for first-step sequencing is shown. *In situ* sequencing defines cluster coordinates, which are modified to expose oligo-dT for RNA capture. Tissue sections are placed on the array and captured RNAs are reverse transcribed into spatially barcoded cDNA, followed by library preparation and sequencing. (c) Schematic of the Stereo-seq spatial transcriptomics workflow. The technique uses a patterned chip consisting of DNA nanoballs, each tagged with a unique coordinate identity (CID) barcode. Oligonucleotide probes containing unique molecular identifiers and poly(dT) sequences hybridize to the DNA nanoballs for targeted mRNA capture from tissue sections.

A meaningful approach to address such a limitation was introduced by Fan *et al.* as expansion spatial transcriptomics (Ex-ST).[47] By physically enlarging tissue samples *via* expansion microscopy, both transcript availability and spatial resolution of array-based spatial transcriptomics can be enhanced. With an effective resolution to ~20 μm per spot, more precise cell-level transcript detection was enabled, even their subcellular localization in specific cell types such as neurons.

Later innovations in NGS-based spatial methods, include Slide-seq and Slide-seqV2,[48,49] utilize densely packed DNA-barcoded bead arrays to achieve transcriptome-wide RNA detection in single cells. Upon transferring mRNAs from tissue sections onto these beads, the captured transcripts are reverse-transcribed, amplified, and sequenced. Spatial localization of these RNA molecules can be achieved by decoding the bead-specific barcodes. Slide-seq offers a spatial resolution of ~10 μm,[48] significantly surpassing Visium and Ex-ST. Nearly a 10-fold increase in RNA capture efficiency and transcript detection per bead was achieved in the improved version Slide-seqV2, making it an attractive platform for high-resolution spatial transcriptomics.[49] By incorporating expansion microscopy into Slide-seqV2, it may hold promise to further enhance resolution and detection sensitivity beyond current capabilities.

Seq-Scope, developed by the Lee group, is another intriguing approach to improve the spatial resolution of NGS-based RNA profiling.[50] It employs a two-step sequencing strategy, with an initial round of sequencing to map randomly barcoded oligonucleotide clusters immobilized on an Illumina solid surface and a second sequencing round to identify transcript sequences after RNA capture (Fig. 3b). Seq-Scope can achieve an impressive inter-cluster distance of ~0.5–0.8 μm, allowing for near-subcellular resolution spatial RNA analysis.[50]

Another notable platform is Stereo-seq, developed for spatial transcriptomics across large-scale tissue architectures including whole embryos.[51] Stereo-seq utilizes patterned nanoarrays of DNA nanoballs,[52] embedded with spatial barcodes and capture sequences, arranged on a lithographically etched silicon chip with fields of view ranging from 1 cm^2 to over 13 cm^2 (Fig. 3c). With submicron size spots and inter-spot distances, Stereo-seq enables transcriptomic profiling at an unprecedented spatial scale at single-cell or even subcellular resolution.

These examples together have underscored the advancements and transformative potential of NGS-based spatial transcriptomics. Through continued improvements in separation techniques and surface chemistry, the spatial resolution and transcript detection efficiency of these platforms can be further enhanced, providing powerful tools for dissecting cellular diversity, gene expression heterogeneity, and tissue organization with great details and high throughput.

We need to mention that many of these above discussed spatial transcriptomics technologies generate increasingly complex and high-dimensional datasets, necessitating computational models for signal decoding, error correction, and biological interpretation.[53] For instance, in DART-FISH, large-scale RNA imaging was paired with computational deconvolution and decoding to achieve single-cell resolution gene profiles across human tissue.[31] SEDR integrates spatial and transcriptional data using autoencoders and variational graph embeddings to improve clustering and visualization of single-cell niches.[54] Graph signal processing methods such as SpaGFT apply Fourier transforms on tissue graphs to identify spatially variable genes and enhance domain annotation.[55] As this review focuses more on the chemical probe development, we only try to use these examples to illustrate how computational modelling can also be a central enabler for scalable, accurate, and interpretable multiplexed RNA imaging. We would like to refer the audiences who are interested in learning more about these fixed sample spatial transcriptomics techniques to some recent excellent reviews elsewhere.[56–59]

3 Multiplexed RNA imaging in living cells

The above-discussed techniques are valuable tools for detecting transcriptional heterogeneity among isogenic and various cell populations. However, because these methods require cell fixation and permeabilization, they cannot capture temporal changes in RNA levels or dynamic molecular events in real time. Considering the RNA lifecycle encompasses a series of tightly regulated and highly interconnected steps in transcription, processing, transportation, localization, translation, and degradation, visualizing these RNA molecules in live cells is very crucial for unravelling the dynamic processes, correlations, and functional roles of RNAs within the complex intracellular environment. There is a strong need for live-cell RNA imaging technologies with high spatial and temporal resolution, and ideally with high throughput capability. In this section, we will review key recent advances for multiplexed RNA imaging in living cells.

3.1 Synthetic oligonucleotide-based probes

In vitro synthesized nucleic acid-based probes are powerful tools for imaging intracellular RNA distributions. On one hand, RNAs of interest can be directly synthesized and labeled with fluorophores *in vitro*, followed by microinjection or delivery into the cells.[60] On the other hand, by simply tuning their sequences, nucleic acids can also be programmed to recognize specific endogenous target RNAs through predictable base pairing and *in situ* hybridization. These synthetic oligonucleotide probes can be biocompatible, capable for precise chemical modification, and exhibit modular and versatile architectures, which make them particularly attractive for RNA sensing.

Fluorophore-labeled single-stranded DNA probes, such as molecular beacons (MBs), mark a simple but capable tool for such a purpose. MBs are stem-loop-structured oligonucleotides, labeled with a reporter fluorophore and a quencher. Upon hybridization with target sequences, the hairpin structure unfolds, leading to fluorescence generation with minimal background (Fig. 4a). Since its initial development in 1996,[61] MBs have been widely used for *in vitro* and intracellular RNA detection. By labelling MBs with fluorophores of distinct colors, simultaneous and real-time visualization of multiple RNA

species have been achieved inside living cells.[62,63] However, live-cell imaging beyond two or three RNA targets remains a common technical challenge for these MB probes, due to limitation in available spectrally distinct fluorophores.

The Tang group developed a four-color nanoprobe based on MBs and gold nanoparticles (AuNPs).[64] These AuNPs were functionalized *via* gold–thiol bonds to anchor four different MBs, each specific to one cancer-associated mRNA. In the absence of target mRNAs, the fluorophores remain in close proximity to the AuNPs, resulting in efficient fluorescence quenching (Fig. 4b). When the target mRNAs are present, DNA–RNA hybridization unfolds the hairpin and separates the fluorophores from the AuNP surface to restore fluorescence signals. Without requiring additional small-molecule quenchers and being effectively internalized by the cells, these AuNPs can also facilitate the cellular delivery of oligonucleotide probes.

Beside molecular beacons, oligonucleotide probes can also be engineered to fold into other defined nanostructures for sensitive and multiplexed RNA imaging in living cells. One such example is based on self-assembled DNA tetrahedral structures, which can spontaneously enter the cells and remain intact inside living cellular environment.[65–67] Several DNA tetrahedron-based probes have been employed for multiplexed live-cell RNA detection. The Xiang group developed a self-assembled four-strand DNA tetrahedral nanostructure, incorporating two hairpin probes.[68] Each hairpin was labeled with a distinct fluorophore-quencher pair and designed to detect a target microRNA, *e.g.*, miRNA-21 and miRNA-155. Similarly, the Willner group positioned three hairpin probes along the edges of DNA tetrahedron, enabling concurrent cellular imaging of three miRNAs, *e.g.*, miRNA-21, miRNA-221 and miRNA-155.[69] The vertices of the DNA tetrahedron can also be fused with duplex extensions for multiplexed RNA detection, as demonstrated by the Zhang group for simultaneously detecting three tumor-related mRNAs, including *c*-myc, TK1 and GalNAc-T.[70]

Beyond DNA tetrahedrons, other complex nanostructures, such as DNA triangular prisms (DTPs), have also been employed for multiplexed RNA imaging. In one design, two pairs of metastable catalytic hairpin assembly (CHA) probes, an AS1411 aptamer, and a biotinylated DNA strand were positioned at distinct vertices of the DTP,[71] which components were further assembled *via* streptavidin to form multivalent DTPs (SA-DTPs) for miRNA imaging in MCF-7 cells. Upon binding to a target miRNA, mono-DTP initiated a localized CHA reaction and released the target miRNA, which could then be rapidly

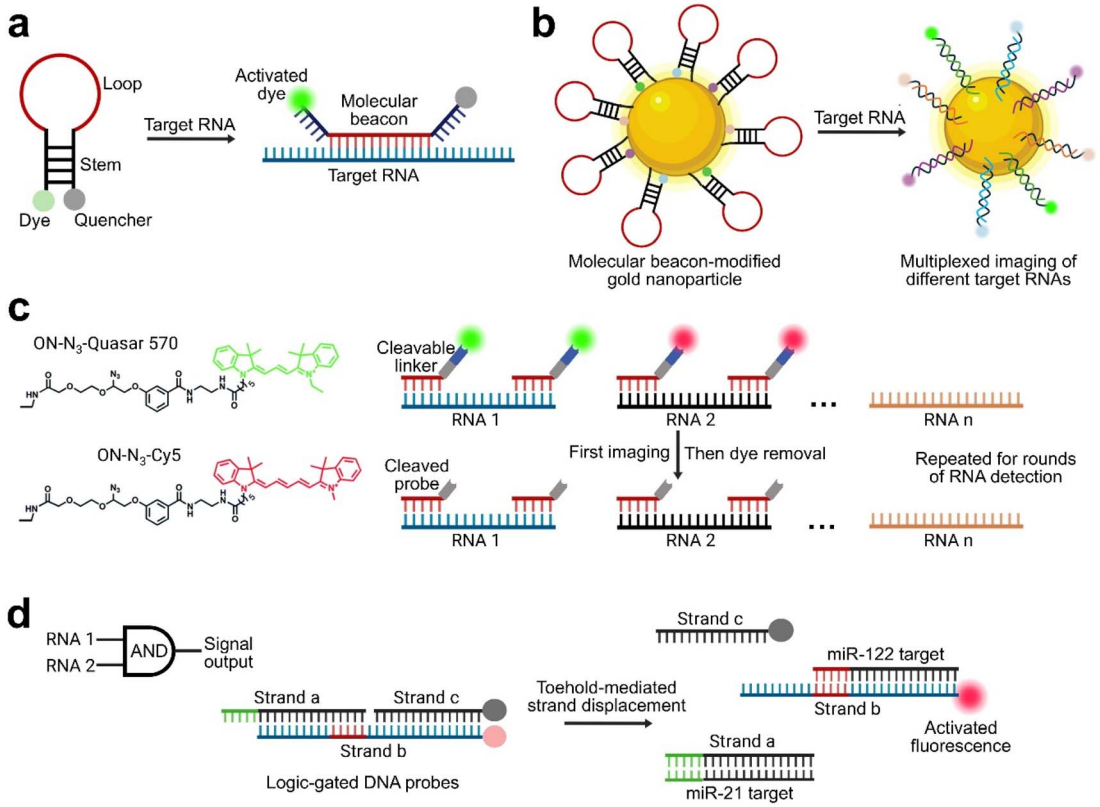

Fig. 4 (a) Molecular beacon-based single-stranded oligonucleotide probes that can generate fluorescence signals upon hybridization with a target RNA sequence. (b) A multi-color molecular beacon-modified gold nanoparticle probe system for the simultaneous detection of multiple intracellular RNAs. In the absence of target RNA, the fluorophores are near to the surface of gold nanoparticle with a quenched fluorescence signal, which can be recovered by target RNA-induced extension of the DNA probes. (c) Chemical structures and schematic of biorthogonal cleavable oligonucleotides for rounds of *in situ* RNA analysis and imaging. (d) A sample many-to-one Boolean logic AND-gated DNA probes for detecting the co-existence of two microRNAs inside live cells, *via* toehold-mediated DNA strand displacement reactions.

Table 2 Techniques for multiplexed RNA imaging in living cells

Technique	Multiplexing	Resolution	Principle	Advantages	Limitations	Ref.
Molecular beacons probes	Up to 4 RNAs	Can detect at single-molecule level	Hairpin DNA probes fluoresce upon hybridizing target RNA	Simple in design, real-time detection	Limited multiplexing, cell-to-cell delivery variations	62–64
Assembled DNA nanostructures	Up to 3 RNAs	Potentially at single-molecule level	Self-assembled DNA nanostructures with multiple probes	Enhanced stability and self-delivery capability	Limited multiplexing, relatively complex and large structures	68–73
Enzyme-free DNA circuits	<3 RNAs	Subcellular	Strand-displacement circuits amplify signal upon RNA binding	Amplified signal for sensitive RNA detection, potential logic analysis	Limited multiplexing, slow kinetics, risk in off-target activation	76–78
DNA probes + nanomaterials	Up to 4 RNAs	Can detect at single-molecule level	DNA-conjugated nanomaterials for enhanced fluorescence	Improved cellular delivery and stability, high sensitivity, multi-function	Limited multiplexing, potential cytotoxicity	64 and 87–90
Bacteriophage-derived RNA labelling tags	Up to 3 RNAs	Can detect at single-molecule level	Phage RNA tag with FP-fused RNA-binding coat protein	Genetically encoded system, real-time and long-term RNA tracking	Limited multiplexing, requires RNA tagging, background signal	91–96
CRISPR-dCas system	Up to 3 RNAs	Can detect at single-molecule level	Orthogonal FP-fused dCas variants or gRNAs with fluorogenic RNA tags	Target endogenous RNAs, genetically encodable	Limited multiplexing, background signal	101–111
Fluorogenic RNA aptamer probes	Up to 3 RNAs	Can detect at single-molecule level	Orthogonal spectrally distinct light-up RNA aptamer/dye pairs	Small tag, low background, genetically encodable, can target endogenous RNAs	Limited multiplexing, moderate brightness	118–129
SeqFRIES	Up to 4 RNAs	Potentially at single-molecule level	Orthogonal fluorogenic RNA aptamer/dye pairs with sequential imaging	Small tag, low background, genetically encodable, can target endogenous RNAs	Limited multiplexing, time needed for repeated cycles	128
RNA-stabilized protein tags	Up to 4 RNAs	Can detect at single-molecule level	RNA recruits FP *via* RNA-binding motifs for fluorescence	High signal-to-noise ratio, genetically encodable	Limited multiplexing, often requires RNA tagging	131–133

recaptured by adjacent mono-DTPs *via* spatial confinement effect, triggering additional CHA cycles with amplified fluorescence signals. Dual-color cascade has been further engineered for simultaneous detection of two types of miRNAs in living cells.

Various self-assembled nucleic acid nanostructures have been reported already, including intricate DNA polyhedral and origami.[72,73] For the purpose of RNA imaging, an ideal nanostructure should self-internalize into the cells and remain stable for at least several hours. The incorporation of modified nucleotides, such as locked nucleic acids and phosphorothioate backbones,[74] may be considered. Here, the stability includes both resistance towards enzymatic degradation and intactness of self-assembly inside varied cellular environment. Meanwhile, if the goal is to apply these oligonucleotide-based probes to image a large variety of RNAs in living cells, stripping of the probes after one round of imaging may be needed. In this case, relatively less stable DNA nanostructures or biorthogonal cleavable oligonucleotides (Fig. 4c)[75] could be preferred. Similar to what has been shown in MERFISH or seqFISH, iterative delivery and hybridization cycles of these functional oligonucleotide probes in living cells potentially can be used for imaging different RNA species at high throughput.

These DNA probes can also be incorporated with isothermal enzyme-free DNA circuits, especially the above-mentioned CHA and hybridization chain reaction (HCR).[76,77] However, in terms of multiplexed RNA imaging, such circuit design must be fine-tuned to reduce crosstalk among the circuit. One direction is leveraging many-to-one Boolean logic gates to enhance the multiplexing capacity of cellular RNA detection. For instance, two miRNA targets in a simple AND logic gate can induce a single output fluorescent signal (Fig. 4d).[78] As a result, 2–4 spectrally distinct fluorophores could be theoretically applied for the profiling of ≥4–8 target RNAs. While the construction of more robust DNA circuits that function inside cells still is a technical challenge.

Synthetic bioorthogonal fluorogenic oligonucleotide probes are another type of powerful tools that allow dynamic, multiplexed, and single-molecule-level RNA imaging in living systems.[79–82] Represented by tetrazine-mediated fluorogenic reactions, target RNAs can function as the template to induce the close proximity of a caged fluorophore-labeled oligonucleotide probe and another tetrazine-modified strand. Tetrazine-triggered uncaging reactions could then induce a turn-on fluorescence, yielding a wash-free and live-cell-compatible RNA detection system with minimal background signals.[79–82] Hybrid strategies that combine nucleic-acid amplification or catalytic hairpin circuits with fluorogenic bioorthogonal steps have also been reported, offering enhanced specificity and stronger signal output for RNA imaging.[83] Similarly, approaches that merge metabolic labelling of nucleosides with fast fluorogenic ligations have also been reported.[84–86] Even though, to the best of our knowledge, these bioorthogonal fluorogenic oligonucleotide probes have been barely used for multiplexed RNA detection in living cells, we would like to still highlight these approaches here as in principle they can indeed expand the chemical space for multiplexing.

Lastly, oligonucleotide-based multiplexed RNA imaging probes can be functionalized on nanomaterials, such as graphene oxide (GO),[87,88] gold nanoparticles,[64,89] and magnetic nanoparticles,[90] *etc.* Unlike pure DNA-based scaffolds, these nanomaterials possess additional inherent fluorescence quenching and adsorption properties or can function as delivery vehicles to improve the intracellular transportation and stability of the oligonucleotide probes (Table 2). Another notable feature of oligonucleotide-nanomaterial complexes is that beyond RNA detection and imaging, they can also serve as multi-functional platforms,[75] for example, to achieve targeted drug delivery and therapeutics in personalized medicine.

3.2 Bacteriophage-derived RNA labelling tags

When using the above-discussed synthetic oligonucleotide probes for cellular RNA imaging, probes' cellular penetration, specificity of delivery, spatial and temporal variation in cellular concentration, and long-term stability are still potential concerns. In contrast, several genetically encodable fluorescent probes have been engineered to overcome these challenges. One popular genetically encoded RNA imaging platform is based on RNA-binding coat proteins derived from bacteriophages. In such a system, RNAs of interest are tagged with phage RNAs, such as MS2, PP7, and boxB, which can be imaged inside cells *via* co-expressed fluorescent protein-fused corresponding RNA-binding proteins, *e.g.*, MS2 coat protein (MCP), PP7 coat protein (PCP), and λN peptide (Fig. 5a). The first usage of these tags for dual-color live-cell RNA imaging was reported by the Jansen group,[91] where boxB-tagged ASH1 mRNA and MS2-tagged IST2 mRNA were visualized in yeast *via* GFP-λN and RedStar-MCP signals, respectively.

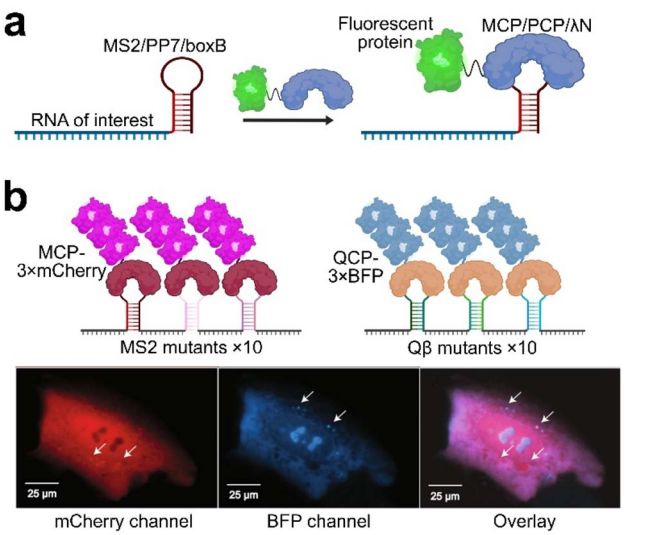

Fig. 5 (a) Schematic illustration of bacteriophage-derived RNA labelling tags for live-cell multiplexed RNA imaging. RNAs of interest with MS2, PP7, boxB RNA tags can be specifically recognized and visualized by fluorescent protein-conjugated MS2 coat protein (MCP), PP7 coat protein (PCP), or boxB coat peptide. (b) Simultaneous RNA imaging in U2OS cells based on an MS2/MCP and Qβ/QCP orthogonal pairs. Cell images were reproduced from ref. 96 with permission from the authors and Springer Nature, copyright 2021.

A more prevalent MS2/MCP and PP7/PCP system for simultaneous visualization of two RNA transcripts was later introduced by the Singer group. By fusing two MDN1 alleles respectively with 24 copies of MS2 or PP7 RNA hairpins at the 3′ untranslated region (3′ UTR), simultaneous monitoring of two distinct mRNAs was achieved at the single-molecule level in living yeast cells.[92] The Levine group further demonstrated that such MS2 or PP7 repeats can also be used in Drosophila embryos to study the relationship between enhancer–promoter interactions and transcriptional bursting,[93] and the dynamic expression patterns of the pair-rule genes even-skipped (eve) and fushi tarazu (ftz) during early embryogenesis.[94] It is worth noting that bacteriophage-derived RNA labelling tags have been continually evolved to improve their properties for live-cell RNA imaging. As an example, a key improvement to the MS2/MCP system was achieved by Tutucci *et al.* for tracking short-lived mRNAs in living cells,[95] which has enabled the dynamic measurement of the entire mRNA life with minimal perturbation.

Another bacteriophage-derived Qβ/QCP (Qβ coat protein) RNA/protein pair has also been used for orthogonal and multiplexed RNA imaging. The Amit group applied a high-throughput approach that combined oligonucleotide library screening with machine learning to design RNA cassettes that specifically bind to MCP, PCP and QCP.[96] Such designed cassettes can enable simultaneous multiplexed RNA imaging in U2OS mammalian cells without cross-reactivity (Fig. 5b). These high-affinity RNA/coat protein pairs have increased our ability to develop genetically encodable tools for cellular RNA imaging and regulation. To enable highly multiplexed RNA detection in living systems, screening and identification of additional orthogonal RNA/coat protein pairs is still largely needed.

3.3 CRISPR-dCas systems

Clustered regularly interspaced short palindromic repeats (CRISPR) and their associated endonucleases (Cas) have been widely used in gene editing.[97,98] Catalytically inactive variants, CRISPR-dCas, can also be repurposed as programmable tools for nucleic acid tracking and live-cell imaging of specific DNAs or RNAs.[99,100] Unlike the above-mentioned MS2/PP7/Qβ tags that require genetic engineering of the target RNAs, CRISPR-dCas systems can directly image endogenous RNAs in living cells. In such system, by fusing dCas with fluorescent proteins or modifying synthetic dyes onto designed guide RNA (gRNA) or CRISPR RNA (crRNA), cellular RNAs can be tracked through sequence-specific recognition. This modular system allows flexible target switching simply by replacing the gRNA/crRNA, enabling broad target coverage and facilitating dynamic studies of RNA localization and function in living cells.

Several studies have applied the CRISPR-dCas13 system for multi-color and dynamic RNA visualization in living cells. For instance, the Qi group developed a CRISPR live-cell fluorescent *in situ* hybridization (LiveFISH) technique, utilizing fluorescently labeled oligonucleotides for tracking genomic loci and RNA transcripts across various cell types.[101] By integrating dCas13 with dCas9 systems, LiveFISH enables the simultaneous real-time visualization of genomic DNA and its corresponding RNA transcript in live U2OS cells.

The Chen group applied two orthogonal dCas13 variants (PspCas13b and PguCas13b) to enable dual-color imaging of two RNA species (*e.g.*, NEAT1 and SatIII).[102] Various CRISPR-Cas13 proteins have also been systematically screened, unfortunately, no additional dCas13 candidates was identified as suitable for orthogonal RNA labelling.[103] Inspired by the CRISPRainbow strategy,[104] an alternative approach, termed CRISPRpalette, was further developed by the Chen group to simultaneously visualize multiple RNAs by integrating each gRNA sequence with an above-mentioned orthogonal MS2 and PP7 RNA tag (Fig. 6).[103] Triple-color RNA imaging was then demonstrated in HeLa cells by adding an additional orthogonal RNA/peptide tag (*i.e.*, pepper/tDeg as explained in details later in Section 3.5) to enable simultaneous detection of MUC4, NEAT1_2, and SatIII.

Fluorescent RNA aptamers (will be further discussed in Section 3.4) have also been embedded within dCas13 gRNAs for multi-color RNA imaging, for example, as that shown in the so-called CasFAS system developed by the Zhou group.[105] By embedding β-actin sgRNA with 8 × pepper, MUC4 sgRNA with 2 × broccoli, and NEAT1 sgRNA with 2 × pepper-2 × broccoli, three RNA targets can be discriminated and imaged together in living cells. While the CRISPR/dCas13 system is well-suited for direct imaging of endogenous RNAs, it still faces some key limitations. Notably, there remains a lack of effective design rules for dCas13b crRNAs to target arbitrary RNA sequences,[103,106] and the signal-to-noise ratios of the CRISPR/dCas13b platform is often not high.[102]

As an alternative to dCas13, several other Cas proteins have been adapted for RNA tracking in live cells. For example, with the aid of a single-guide RNA and PAM-presenting oligonucleotide (PAMmer), RNA-targeting dCas9 has been used to image

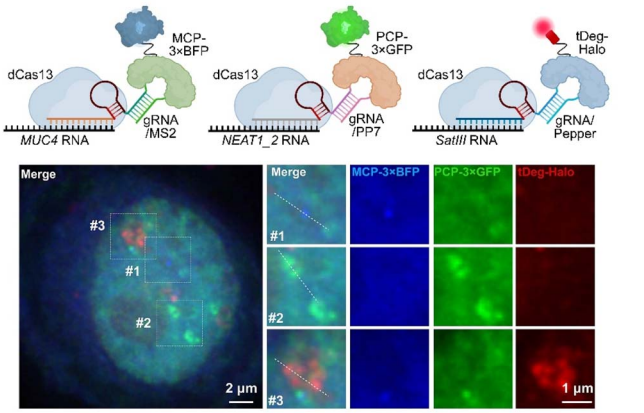

Fig. 6 Schematic illustration of a CRISPR-dCas13 system, CRISPRpalette, for live-cell multiplexed RNA imaging. Simultaneous detection of MUC4, NEAT1, and SatIII RNAs were achieved in living HeLa cells by modifying each corresponding gRNA sequence with a MS2, PP7, or pepper RNA motifs. Then fluorescent protein-tagged MCP and PCP, as well as Halo-tagged Tat peptide were used for orthogonal labelling and multiplexed RNA imaging. Cell images were reproduced from ref. 103 with permission from the authors and Elsevier, copyright 2022.

mRNAs in RNA granules.[107] In one study, Jiang and colleagues developed a CRISPR-based light-up RNA stabilizer (LUSTER) system, which avoids genomic tagging and instead uses dCas9 to stabilize extended guide RNAs that would otherwise undergo rapid degradation.[108] A fluorogenic aptamer is embedded within the misfolded guide RNA scaffold, which only regains the proper conformation upon binding target RNAs, thereby generating a light-up signal. Multiplexed RNA imaging can be achieved through the incorporation of orthogonal fluorogenic aptamers. Compared to dCas13, the CRISPR/dCas9 system normally retains a strong dependence on the protospacer adjacent motif (PAM) and precise sequence targeting with less collateral activity. While the effectiveness of dCas9 platform for visualizing low-abundance RNAs needs further validation. In addition, potential misfolding of the complex guide RNA scaffold may impair its ability to form functional complexes with dCas9.

CRISPR/dCas12a has also been used for live-cell RNA imaging. A notable feature of the dCas12a system is the relatively simple crRNA structure, which enhances the design and proper folding of the platform. For example, by leveraging two orthogonal dCas12a variants, LbCas12a and AsCas12a, Yin's group engineered a dual-RNA imaging platform with high specificity.[109] By fusing these two dCas12a variants to distinct fluorescent proteins (*e.g.*, GFP and OFP), this system enabled simultaneous visualization of Bcl2 mRNA (a breast cancer-related transcript) and piR-36026 (a PIWI-interacting small noncoding RNA) in the same breast cancer cell.

Another CRISPR-based RNA imaging system was recently developed by the Doudna group based on a Type III RNA-targeting CRISPR-Csm complex.[110] In combination with multiplexed crRNAs, fluorescently labeled Csm complexes allow single-molecule imaging of endogenous RNAs in living cells.[111] Individual distinct RNA species, such as NOTCH2 and MAP1B mRNAs can be visualized, highlighting the platform's potential for multiplexed and high-resolution RNA tracking.

With continuous discoveries of new universal and adaptable CRISPR-dCas complexes, additional orthogonal Cas systems can be potentially identified. Different classes/types of Cas proteins may also be combined to enable highly specific multi-color imaging of various endogenous RNAs.

3.4 Fluorogenic RNA aptamer-based probes

Fluorogenic RNAs are RNA aptamers that can bind to specific small-molecule dyes and then activate fluorescence signals at defined wavelengths.[112,113] These RNAs are highly modular and readily engineerable. Over the past decade, a diverse set of fluorogenic RNAs, such as spinach, broccoli, corn, mango, SRB-2, pepper, beetroot, RhoBAST, and squash, *etc.*, have been developed as genetically encoded fluorescent probes for RNA detection and imaging in live cells.[114–116] Some major advantages of fluorogenic RNAs include their high signal-to-background ratio and potential broad choice of synthetic chemical dyes.

Several orthogonal fluorogenic RNA/dye pairs, such as broccoli/DFHBI-1T & DNB/TMR-DN, beetroot/DFAME & corn/DFHO, broccoli/BI & squash/DFHO, broccoli/DFHBI-1T & mango I/YO3-B, DNB/RG-DN & SRB-2/SR-DN,[117–122] have been used for multi-color cellular imaging. For instance, by leveraging a red-emissive pepper/HBC620 and green-emissive squash/DFHBI-1T pair as the imaging modules, the Nie group designed miRNA-induced light-up RNA sensors based on toehold-mediated strand displacement.[123] Sensitive dual-color imaging of miRNAs (*e.g.*, miR-21 and miR-122) was achieved within living cells.

To expand the toolbox of bio-orthogonal fluorogenic RNAs with distinct spectral properties, a large Stokes shift *Clivia*/NBSI RNA/dye pair was recently developed by Yang and colleagues, which can be combined with pepper/HBC497 to enable an interesting single-excitation, dual-emission platform for simultaneous visualization of sgRNAs and genomic loci in a CRISPR-dCas9 system.[124] Similarly, another single-excitation, dual-emission RNA imaging platform was recently reported by harnessing a spectrally red-shifted mSquash/DFHBFPD complex with broccoli/DFHBI-1T.[125] By further incorporating specific photo-removable cages onto the DFHBFPD and DFHBI-1T chromophores, such a photoactivatable system can be used for precise spatiotemporal dual-color RNA imaging in living cells.

Even with a list of orthogonal fluorogenic RNA/dye pairs to choose from, live-cell imaging beyond two RNA targets remains a technical challenge, mainly due to the spectral overlap of these RNA/dye complexes. In addition to the above-mentioned large-Stokes-shift chromophores, some cyan fluorogenic RNAs have also been reported. For example, *Myosotis*, together with its cognate dye DBT, demonstrates strong compatibility and orthogonality with pepper/HBC530 and *Clivia*/NBSI624,[126] making it a promising tool for three-color fluorescence imaging of RNA in live bacterial cells.

Inspired by the seqFISH and MERFISH techniques (Section 2.1), our group recently developed a multiplexed sequential RNA imaging technique, named as seqFRIES, that can function inside living cells (Fig. 7).[127] In seqFRIES, spectrally overlapped orthogonal fluorogenic RNAs are sequentially visualized through iterative cycles of imaging and stripping. Noncovalent reversibly binding fluorogenic RNA/dye pairs are uniquely suitable for such an approach: RNA aptamers can be genetically encoded to target endogenous RNAs or as a tag for RNA tracking, while cell membrane permeable small-molecule dyes can be easily added or removed for rounds of RNA detections. Indeed, by using orthogonal broccoli/DFHBI-1T, DNB/TMR-DN, corn/DFHO, and pepper/HBC620 pairs, multiplexed imaging of four distinct mRNA targets was achieved *via* seqFRIES.[127]

Considering the potential broad choice of synthetic chemical dyes, together with powerful SELEX (systematic evolution of ligands by exponential enrichment) approach for the selection of new RNA aptamers, many additional orthogonal and functional fluorogenic RNA/dye pairs can be expected. With diverse photophysical properties in terms of their brightness, excitation and emission wavelength (*e.g.*, far-red fluorescent probes), fluorescence lifetime, and anisotropy, *etc.*, these tools may be further combined with vibrational, spectral, and lifetime imaging techniques to enable live-cell imaging of even more

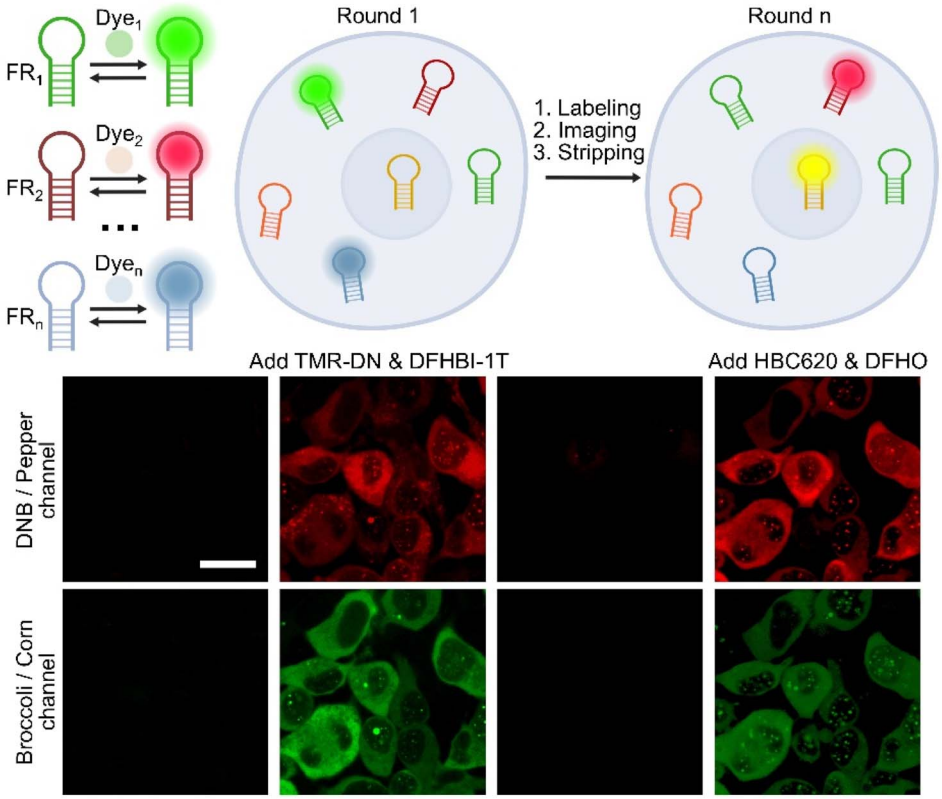

Fig. 7 A sequential fluorogenic RNA imaging-enabled sensor (SeqFRIES) system. Upon specific reversible binding, orthogonal fluorogenic RNA/dye pairs can turn on their fluorescence signals independent from each other. After genetically encoding orthogonal fluorogenic RNAs in living cells, sequential multiplexed detection can be achieved *via* rounds of imaging-and-stripping process by adding and removing the cognate membrane-permeable small-molecule dyes. Shown are the images from HEK293T cell that co-express broccoli, DNB, pepper, and corn fluorogenic RNAs after a sequential incubation with corresponding DFHBI-1T, TMR-DN, HBC620, and DFHO dyes. Scale bar, 15 μm. Reproduced from ref. 127 with permission from the authors and Oxford University Press, copyright 2024.

target biomolecules. For example, by attaching a cobalamin quencher to various fluorophores, a bacterial cobalamin riboswitch-based Riboglow fluorogenic RNA aptamer[128] has recently been repurposed as fluorescence lifetime-based multiplexed imaging probes.[129] In this strategy, cellular RNA targets, *e.g.*, ACTB and a truncated form of NORAD RNA, were tagged with Riboglow variants (Ribo4D and Ribo4A) that exhibit distinct fluorescence lifetimes despite using the same fluorophore, and as a result, allowing orthogonal RNA visualization in the same living cells.

3.5 RNA-stabilized protein tags

Instead of binding specific chemical dyes that are exogenously supplied to the cells, another type of fluorogenic RNA tools have been developed based on RNA-stabilized fluorescent protein tags. The first example of such fully genetically encodable tags was reported by the Jaffrey group based on a TAR RNA sequence (also named as pepper) that can bind and prevent the degradation of a Tat peptide-fused degron sequence domain (tDeg).[130] By appending tDeg to the C-terminus of a fluorescent protein, minimal fluorescence background was shown due to rapid degradation of the protein inside cells. While in the presence of pepper-tagged target RNAs, fluorescent proteins can be stabilized to generate RNA-specific fluorescence signals, enabling cellular RNA imaging at the single-molecule level (Fig. 8a).

Compared to chemical dye-based fluorogenic RNAs, such fully genetically encoded pepper/tDeg system can be potentially more useful for *in vivo* applications, without worrying about possible issues with the dye delivery, biological distributions, nonspecific activation or toxicity. On the other hand, compared to the above-mentioned bacteriophage-derived RNA labelling tags, like the MS2/MCP system, pepper/tDeg can provide a much higher signal-to-background ratio due to the removal of excess unbound fluorescent proteins *via* rapid cellular degradation. As a result, these RNA-stabilized fluorescent protein tags can be a powerful tool for sensitive and robust cellular RNA imaging.

Very recently, three different groups have independently reported new orthogonal RNA-stabilized tags for multiplexed RNA imaging in living systems. The Wu lab developed two additional RNA imaging platforms, termed “mDeg” and “pDeg”, based on the MS2/MCP and PP7/PCP pairs, respectively.[131] Similar to the design of pepper/tDeg, mDeg and pDeg also incorporate a Arg–Arg–Arg–Gly degron sequence to the MCP and PCP proteins. While the native C-termini of MCP and PCP were spatially distant from their RNA-binding sites, circular permutation was

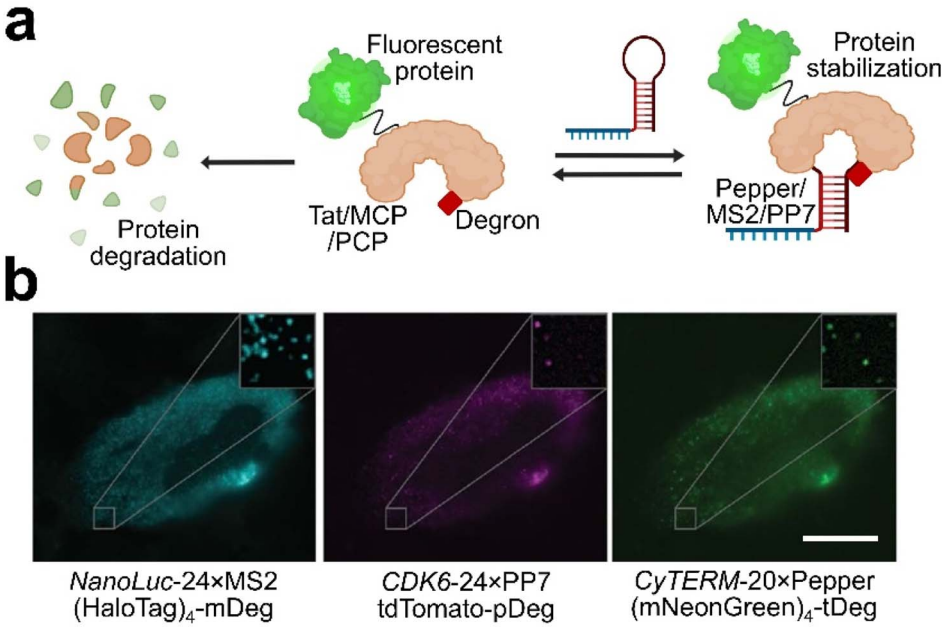

Fig. 8 (a) Schematic illustration of RNA-stabilized protein tags for live-cell RNA imaging. A protein destabilization degron domain is appended to the C-terminus of fluorescent protein-tagged Tat peptide or MS2/PP7 coat protein to induce protein degradation. While in the presence of a cognate pepper, MS2, or PP7 RNA motif, the degron can be shielded and thus stabilize the protein to generate localized fluorescence signals. (b) Orthogonal imaging of three different RNA species in live U2OS cells using MS2-mDeg (degron-appended MCP), PP7-pDeg (degron-appended PCP) and pepper-tDeg (degron-appended Tat peptide). Scale bar, 20 μm. Reproduced from ref. 131 with permission from the authors, copyright 2024.

employed to reposition the degron proximal to the MS2- and PP7-binding interface. These newly engineered MS2/mDeg and PP7/pDeg systems are fully orthogonal, not only to each other but also to the original pepper/tDeg platform, thereby enabling three-color RNA imaging in living cells (Fig. 8b).

Quite similarly, through circular permutation and attaching C-terminal degron, the Ngo group also developed conditionally stable variants of the MCP and PCP proteins to reduce background fluorescence in live-cell RNA imaging.[132] Dual-color mRNA imaging was also achieved with single-molecule sensitivity. In another work, the Jiang group extended this concept to additional RNA-binding proteins, including L7Ae that recognizes Box C/D RNA, Cse3 for EcCBS RNA motif, and LIN28A that recognizes Let7d RNA.[133] *Via* the development of these orthogonal RNA-stabilized fluorogenic reporters, an impressive four-color, live-cell multiplexed RNA imaging platform was demonstrated using fluorogenic Cerulean-fLIN28A, EGFP-fL7Ae, tdTomato-fMCP, and iRFP670-fCse3. With superior signal-to-background ratio and high sensitivity, these genetically encodable fluorogenic RNA tags can potentially be widely used for cellular RNA imaging.

4 Applications of multiplexed RNA imaging tools for understanding RNA biology and diseases

Advances in multiplexed RNA imaging and spatial transcriptomics techniques have greatly increased our abilities for studying gene expression processes from transcription, modifications, and translation to various RNA-involving interactions and degradation. For instance, MERFISH and seqFISH+ have been utilized to investigate how 3D genome organization can influence transcriptional activities. In this case, a modified version of seqFISH+ was designed to target intronic regions of >10 000 genes, revealing that nascent transcription sites tend to localize on chromosome surfaces.[15] By combining MERFISH (for transcriptomic imaging), DNA-MERFISH (for mapping chromatin structure), and immunofluorescence (for imaging nuclear components), the Zhuang group simultaneously visualized over 1000 gene loci and their nascent transcripts, indicating the correlations between localized chromatin compartments and their transcription activities (Fig. 9a).[134]

Multiplexed subcellular RNA imaging techniques also provide insights into transcriptional regulation and processing. For example, pooled genomic screening has been paired with RNA imaging to evaluate the roles of various transcriptional activators and repressors.[135] The transcription and splicing processes were also observed together *via* multi-color imaging by tagging introns and exons with the MS2/MCP and PP7/PCP system, revealing an interesting coordination effect governed by a kinetic competition process (Fig. 9b).[136] Findings from these imaging tools also demonstrated that splicing can occur over a wide timescale, ranging from ~20 seconds to several minutes. Alternative splicing appears to be stochastic at the single-cell level, varying significantly from one cell to another.[137]

Innovative multiplexed live-cell imaging tools have also contributed for studying translation kinetics and RNA stabilities. The Chao group developed a TRICK probe that utilizes dual

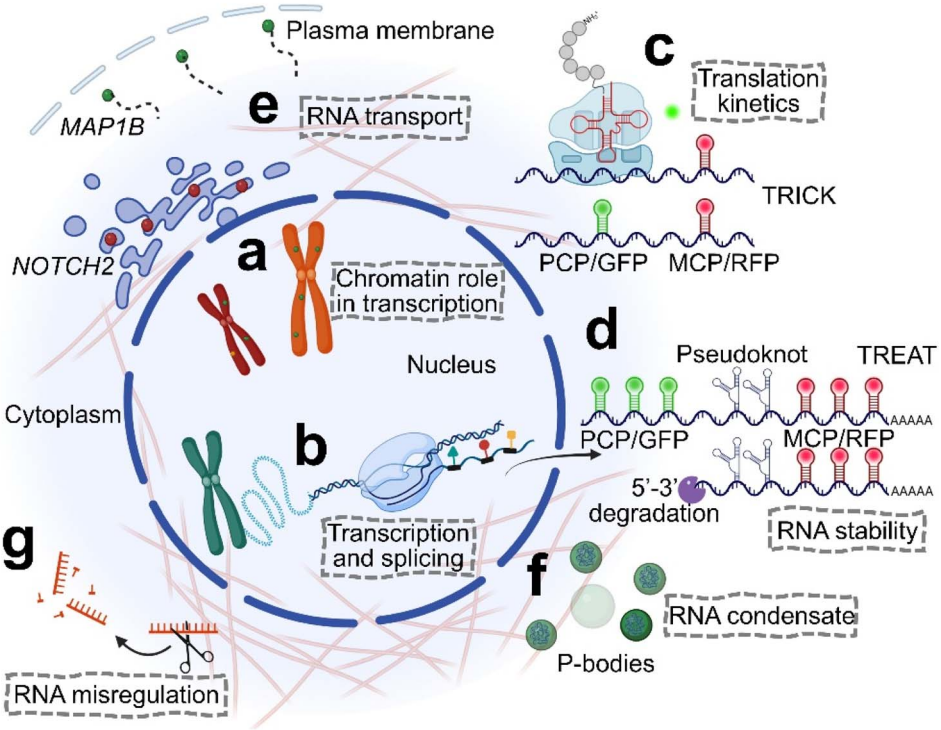

Fig. 9 Highlights of multiplexed RNA imaging usage for exploring RNA biology and diseases. (a) Integrated imaging approaches reveal that nascent transcription sites localize preferentially on chromosome surfaces (green dots), highlighting correlations between chromatin compartmentalization and transcriptional activity. (b) Simultaneous imaging of transcription and splicing reveals a coordinated kinetic competition between two processes. (c) TRICK assay visualizes translation initiation and kinetics on single mRNAs using MS2/MCP and PP7/PCP dual reporter systems. (d) TREAT biosensor design for monitoring mRNA turnover. By combining MS2 and PP7 stem loops with viral pseudoknot elements that block degradation, dual-labeled intact transcripts can be distinguished from single-labeled stabilized degradation intermediates in living cells. (e) Live-cell RNA transport imaging reveals distinct transport pathways such as ER-localized NOTCH2 transcripts and peripheral-directed MAP1B transcripts. (f) Phase-separated RNA condensates such as stress granules and P-bodies regulate RNA storage, sorting, and decay. (g) Multiplexed RNA imaging enables real-time tracking of RNA dynamics, providing insights into viral infections, cancer, and neurodegenerative diseases that are relevant to RNA misregulation and aberrant metabolism.

RNA labelling to enable direct visualization of translation initiation on individual mRNA molecules (Fig. 9c).[138] mRNA translation was found to initiate rapidly upon RNA export into the cytoplasm, rather than in the nucleus. To further dissect mRNA turnover dynamics, another MS2/MCP and PP7/PCP-based orthogonal RNA imaging approach, called TREAT, was developed to distinguish between intact and degrading transcripts in real time (Fig. 9d).[139] Cellular mRNA degradation was revealed as a continuous process, not by bursts, and that the majority of cytoplasmic decay occurs outside of P-bodies.[140]

Current imaging techniques have also enabled the direct observation of RNA transport within cells. For example, by incorporating the CRISPR-Csm system with multiplexed guide RNAs, single-molecule live-cell fluorescence *in situ* hybridization (smLiveFISH) was applied to visualize individual mRNA molecules in real time (Fig. 9e).[111] Distinct transportation mechanisms and pathways of different RNAs have been revealed, including translation-dependent localization of NOTCH2 mRNA to the endoplasmic reticulum and directional movement of MAP1B mRNA toward the cell periphery.

Indeed, the spatial organization of RNAs within cells is a critical determinant of their functional output. For example, by profiling the localization of transcripts from thousands of genes, MERFISH revealed that mRNAs encoding secreted proteins are enriched at the endoplasmic reticulum, and that nuclear-to-cytoplasmic RNA ratios can serve as indicators of cell cycle states.[16] In polarized cells, such as those in the intestinal epithelium, asymmetric mRNA localization modulates translational efficiency; while in non-polarized cells, the targeting of transcripts to specific subcellular regions often depends on ongoing local translation.[141] Deep tissue multiplexed RNA imaging methods, such as cycleHCR, further expand these capabilities by enabling the simultaneous visualization of numerous RNA targets with high-resolution in thick tissue samples.[142] Mapping of RNA localization and transport in three dimensions was achieved, providing valuable insights into spatial gene regulation and RNA movement within complex biological environments.

Beyond simple localization, RNA molecules can assemble into phase-separated condensates such as stress granules and P-bodies, for regulating RNA storage, interaction specificity, and decay.[143] Previous imaging work has challenged the traditional view that P-bodies are the primary sites of mRNA degradation, and instead highlighting their roles in RNA sorting and storage

(Fig. 9f).[144,145] Moreover, super-resolution multiplexed RNA imaging approaches have revealed the composition and dynamics of these condensates. Particular mRNAs are selectively recruited into these condensate structures.[146] These findings underscore the complexity of post-transcriptional regulation and indicate that spatial compartmentalization and condensate formation can contribute to the fine-tuning of gene expression.[147] Further investigations may still require the incorporation of multiple advanced RNA imaging techniques with higher throughput and spatiotemporal resolution as discussed in this review.

These emerging multiplexed RNA imaging and spatial transcriptomics technologies are also transforming our ability to study RNA-based molecular foundations of diseases.[148,149] On one hand, the spatial context is essential for complex disease processes as that shown in tumor heterogeneity, tissue remodelling, and immune cell infiltration.[150,151] Spatial transcriptomics has been widely applied in diverse disease models,[148] especially for mapping cancer heterogeneity at high resolution[18] and for revealing molecular heterogeneity associated with neurodegenerative disorders (Fig. 9g).[38]

On the other hand, some spatial transcriptomics techniques such as TEMPOmap[40] have begun to enable time-resolved RNA profiling. Emerging live-cell multiplexed RNA imaging approaches further provide real-time dynamic information for monitoring various RNA molecules in disease processes. For instance, CRISPR-dCas13-based RNA imaging tools have enabled real-time visualization of viral RNAs of severe fever with thrombocytopenia syndrome virus (SFTSV) in live HEK293T cells, offering potential insights into the pathogenesis of SFTSV.[105] RNA mis-localization and aberrant RNA metabolism are also known to play a pathogenic role in cancer and neurodegeneration diseases.[152] These live-cell imaging methods can offer unique abilities to track RNA kinetics, transport, and other dynamic functions. Integrating spatial transcriptomics with live cell multiplexed RNA imaging can thus create a holistic view for identifying spatially restricted RNA signatures and their dynamic variations during disease progression, which could potentially translate into improved biomarkers and targeted therapeutic strategies.

5 Perspective and outlook

During the past decade, we have witnessed the rapid emerging and maturation of various multiplexed RNA imaging techniques, especially for spatial transcriptomic studies in fixed cells and tissues. In comparison, live cell multiplexed RNA imaging is still limited by several technical hurdles. The first challenge is the limited number of fluorophores that can be spectrally distinguished and used for simultaneous imaging, which typically restricts multiplexing to visualize just a few RNA species at once. A more routine use of spectral imaging and unmixing can be helpful here to distinguish each fluorophore's unique spectral fingerprints. Meanwhile, the requirement of orthogonal tags further reduces the possibility of applying these multi-color fluorophores in the above-discussed bacteriophage-derived RNA labelling tag, CRISPR-dCas, fluorogenic RNA aptamer, and RNA-stabilized protein tag platforms. A powerful approach for identifying new orthogonal tags could be achieved by combining high-throughput screening method with machine learning and/or bioinformatics, like how high-affinity Qβ/QCP pair was identified.[95] While sequential imaging and stripping strategies have recently been demonstrated for multiplexed live-cell RNA imaging,[128] considering the lengthy protocol and time requirement, it is still very difficult to apply these methods to reach the multiplexing capacity beyond single-digit number of RNAs. Lab-on-a-chip devices that integrate automated fluidic control with imaging and analysis automation, as that shown in MERFISH and seqFISH, can be potentially useful to improve the efficiency and precision of these live-cell sequential imaging techniques.

In addition, critical single-molecule sensitivity and high spatial resolution features for improving the potential multiplexing capabilities of RNA imaging techniques are often more difficult to achieve in live-cell settings than in fixed samples. Commonly used fixed sample signal amplification, tissue clearing, and expansion methods for improving signal-to-noise ratio and spatial resolution cannot be directly applied for live-cell RNA imaging. For live cell studies, the choices of chemicals and fluorescent probes need to base on their membrane permeability, toxicity, and perturbation on natural cellular behaviors. Meanwhile, photobleaching and the speed of protocol to capture dynamic processes also need to be considered. Moreover, many live-cell imaging techniques require genetic tagging or the delivery of synthetic probes, which can be inefficient or perturb native RNA functions. Some systematic comparison over the sensitivity, photostability, and resolution of available RNA imaging tools can be helpful for guiding the potential choice of probes for multiplexed RNA detections in living cells.

The physical size of these RNA imaging probes will also influence their achievable spatial resolution. Large and bulky fluorescent probes, *e.g.*, those based on fluorescent proteins *versus* chemical dyes, can introduce "spatial offsets", *i.e.*, the linkage errors between the position of actual RNA molecule and the fluorescence signal. As a result, for single-RNA tracking and super-resolution imaging, a small number of short RNA tags with enough brightness is often preferred. For example, short synthetic oligonucleotide probes, like those based on locked nucleic acids, can bring the fluorophores close to the target RNA, enhancing localization precision and multiplexing accuracy. Small-sized imaging probes can also be more easily delivered or genetically incorporated into the cells. As compared to miniatured molecular beacon and fluorogenic RNA probes, the further identification and application of small-sized fluorescent protein-tagged dCas system and bacteriophage-derived RNA-binding proteins is still highly needed.

Variations in the cellular abundance of the RNA targets will also affect the choice of imaging techniques. Imaging endogenous low-abundance RNAs without genetic modification remains a major hurdle. Background signals from unbound probes and nonspecific binding will reduce the sensitivity of the imaging approach. Imbalanced probe delivery and expression complicate quantitative analysis, and there is a persistent need

for minimally invasive and real-time imaging methods that do not disrupt cellular physiology. While for large-abundance RNA targets or in regions with high transcript density, optical crowding can lead to overlapping signals, making it difficult to accurately detect and quantify individual RNAs. Additionally, achieving high-resolution quantitative RNA imaging across a large-volume biological sample further increases the technical requirement.

Even with these existing challenges, we expect the future of multiplexed RNA imaging to be still promising. Integration of spatial transcriptomic techniques with multiplexed protein and DNA detection will likely become more routine, allowing multi-omics analyses that correlate RNA, protein, and genomic features within the same cell and tissue context. Improvements in tissue clearing, expansion microscopy, and high-speed imaging are anticipated to facilitate transcriptomic mapping in three-dimensional tissues and even in whole organisms, moving beyond traditional two-dimensional cultures.

We expect many additional systems can be designed for live-cell multiplexed RNA imaging, such as the modular PUM-HD (Pumilio Homology Domain) platform that can programmably recognize specific 8-nucleotide RNA sequences.[153–155] Meanwhile, with the identification of additional orthogonal fluorogenic RNA aptamer/dye pairs and other RNA labelling tags, together with improved sequential imaging and single-molecule detection protocols, the number of RNA species that can be tracked in real time in living systems could be significantly expanded. To increase the sensitivity of existing RNA imaging platforms, some recently emerged genetically encodable RNA circuits can be incorporated.[156,157] In addition, more effective probe delivery approaches, new *in situ* dye-labelling chemistry, as well as the development of biocompatible live-cell clearing and expansion techniques could all be expected to allow advanced multiplexed RNA imaging in living systems.

It is also worth mentioning that cellular high-dimensional molecular signatures obtained *via* these multiplexed imaging techniques, if not used properly, could raise significant security, privacy, and ethical concerns. These RNA signatures may reveal disease states or identity-linked biomarkers, enable covert biosurveillance or misuse, and produce large datasets vulnerable to unauthorized access or re-identification.[158] Especially spatial transcriptomic data from human samples pose additional challenges for consent and governance, as molecular profiles may remain traceable to individuals even after de-identification.[159] In addition, biosafety concerns arise when using genetically encoded tools such as CRISPR, particularly regarding their off-target effects, viral delivery, and/or unintended cellular impacts. Standardized frameworks have been proposed for data and metadata sharing, emphasizing controlled access and reproducibility while safeguarding privacy.[141] Complementary proposals for secure data-sharing architectures also underscore the importance of preventing dual-use and misuse of sensitive transcriptomic datasets through technical obfuscation and tiered access models.[160]

Ultimately, the field is also moving toward minimally invasive, non-fluorescence, and label-free methods capable of visualizing native RNA molecules in more physiologically relevant three-dimensional cultures and *in vivo* models. These methods will greatly enhance our ability to study gene profiles in real time and in complex biological environments. The development of high-throughput RNA imaging platforms is also useful for the functional studies of non-coding RNAs and for potential biomarker screening. Moreover, new approaches combining live-cell RNA imaging with simultaneous visualization of proteins and genomic loci can further provide a more holistic view of these critical molecular interactions and dynamics throughout the whole cellular systems.

Author contributions

All of the authors together conceived the outline of this perspective. L. M. and S. K. wrote the original draft of the manuscript, which was further developed and edited by M. Y.

Conflicts of interest

There are no conflicts to declare.

Data availability

No primary research results, software or code have been included, and no new data were generated or analysed as part of this perspective.

Acknowledgements

The authors gratefully acknowledge the support from Chan Zuckerberg Initiative Dynamic Imaging program (2023-321170), NSF (2435059), and Camille Dreyfus Teacher-Scholar Award to M. Y., and the Society for Laboratory Automation and Screening graduate education fellowship to L. M. The authors also thank other members of the You Lab for useful discussion and valuable comments.

References

1 K. V. Morris and J. S. Mattick, *Nat. Rev. Genet.*, 2014, **15**, 423–437.
2 L. Statello, C. Guo, L. Chen and M. Huarte, *Nat. Rev. Mol. Cell Biol.*, 2021, **22**, 96–118.
3 S. Das, M. Vera, V. Gandin, R. H. Singer and E. Tutucci, *Nat. Rev. Mol. Cell Biol.*, 2021, **22**, 483–504.
4 P. V. Ryder and D. A. Lerit, *Traffic*, 2018, **19**, 496–502.
5 J. Wang, M. Horlacher, L. Cheng and O. Winther, *Briefings Bioinf.*, 2023, **24**, bbad249.
6 P. Yin, S. Kuang and Z. Nie, *Anal. Sens.*, 2022, **3**, e202200090.
7 Y. Xia, R. Zhang, Z. Wang, J. Tian and X. Chen, *Chem. Soc. Rev.*, 2017, **46**, 2824–2843.
8 E. Braselmann, C. Rathbun, E. M. Richards and A. E. Palmer, *Cell Chem. Biol.*, 2020, **27**, 891–903.
9 D. S. Seferos, D. A. Giljohann, H. D. Hill, A. E. Prigodich and C. A. Mirkin, *J. Am. Chem. Soc.*, 2007, **129**, 15477–15479.

10 A. Passaro, M. A. Bakir, E. G. Hamilton, M. Diehn, F. Andre, S. Roy-Chowdhuri, G. Mountzios, I. I. Wistuba, C. Swanton and S. Peters, *Cell*, 2024, **187**, 1617–1635.
11 H. Schwarzenbach, D. S. B. Hoon and K. Pantel, *Nat. Rev. Cancer*, 2011, **11**, 426–437.
12 C. Badowski, B. He and L. X. Garmire, *npj Precis. Oncol.*, 2022, **6**, 40.
13 K. H. Chen, A. N. Boettiger, J. R. Moffitt, S. Wang and X. Zhuang, *Science*, 2015, **348**, aaa6090.
14 E. Lubeck, A. F. Coskun, T. Zhiyentayev, M. Ahmad and L. Cai, *Nat. Methods*, 2014, **11**, 360–361.
15 S. Shah, E. Lubeck, W. Zhou and L. Cai, *Neuron*, 2016, **92**, 342–357.
16 C. Xia, J. Fan, G. Emanuel, J. Hao and X. Zhuang, *Proc. Natl. Acad. Sci. U. S. A.*, 2019, **116**, 19490–19499.
17 S. Shah, Y. Takei, W. Zhou, E. Lubeck, J. Yun, C.-H. L. Eng, N. Koulena, C. Cronin, C. Karp, E. J. Liaw, M. Amin and L. Cai, *Cell*, 2018, **174**, 363–376.e16.
18 P. L. Ståhl, F. Salmén, S. Vickovic, A. Lundmark, J. F. Navarro, J. Magnusson, S. Giacomello, M. Asp, J. O. Westholm, M. Huss, A. Mollbrink, S. Linnarsson, S. Codeluppi, Å. Borg, F. Pontén, P. I. Costea, P. Sahlén, J. Mulder, O. Bergmann, J. Lundeberg and J. Frisén, *Science*, 2016, **353**, 78–82.
19 X. Zhuang, *Nat. Methods*, 2021, **18**, 18–22.
20 S. Tyagi, *Nat. Methods*, 2009, **6**, 331–338.
21 B. A. Armitage, *Curr. Opin. Chem. Biol.*, 2011, **15**, 806–812.
22 R. H. Singer and D. C. Ward, *Proc. Natl. Acad. Sci. U. S. A.*, 1982, **79**, 7331–7335.
23 A. M. Femino, F. S. Fay, K. Fogarty and R. H. Singer, *Science*, 1998, **280**, 585–590.
24 J. M. Levsky, S. M. Shenoy, R. C. Pezo and R. H. Singer, *Science*, 2002, **297**, 836–840.
25 E. Lubeck and L. Cai, *Nat. Methods*, 2012, **9**, 743–748.
26 S. Codeluppi, L. E. Borm, A. Zeisel, G. La Manno, J. A. Van Lunteren, C. I. Svensson and S. Linnarsson, *Nat. Methods*, 2018, **15**, 932–935.
27 G. Wang, J. R. Moffitt and X. Zhuang, *Sci. Rep.*, 2018, **8**, 4847.
28 C. H. L. Eng, M. Lawson, Q. Zhu, R. Dries, N. Koulena, Y. Takei, J. Yun, C. Cronin, C. Karp, G.-C. Yuan and L. Cai, *Nature*, 2019, **568**, 235–239.
29 J. J. L. Goh, N. Chou, W. Y. Seow, N. Ha, C. P. P. Cheng, Y.-C. Chang, Z. W. Zhao and K. H. Chen, *Nat. Methods*, 2020, **17**, 689–693.
30 F. Wang, J. Flanagan, N. Su, L.-C. Wang, S. Bui, A. Nielson, X. Wu, H. T. Vo, X. J. Ma and Y. Luo, *J. Mol. Diagn.*, 2012, **14**, 22–29.
31 K. Kalhor, C. J. Chen, H. S. Lee, M. Cai, M. Nafisi, R. Que, C. R. Palmer, Y. Yuan, Y. Zhang, X. Li, J. Song, A. Knoten, B. B. Lake, J. P. Gaut, C. D. Keene, E. Lein, P. V. Kharchenko, J. Chun, S. Jain, J.-B. Fan and K. Zhang, *Nat. Commun.*, 2024, **15**, 2511.
32 X. Qian, K. Coleman, S. Jiang, A. J. Kriz, J. H. Marciano, C. Luo, C. Cai, M. D. Manam, E. Caglayan, A. Lai, D. Exposito-Alonso, A. Otani, U. Ghosh, D. D. Shao, R. E. Andersen, J. E. Neil, R. Johnson, A. LeFevre, J. L. Hecht, N. Micali, N. Sestan, P. Rakic, M. B. Miller, L. Sun, C. Stringer, M. Li and C. A. Walsh, *Nature*, 2025, **644**, 153–163.
33 E. Denisenko, L. De Kock, A. Tan, A. B. Beasley, M. Beilin, M. E. Jones, R. Hou, D. Ó. Muirí, S. Bilic, G. R. K. A. Mohan, S. Salfinger, S. Fox, K. P. W. Hmon, Y. Yeow, Y. Kim, R. John, T. S. Gilderman, E. Killingbeck, E. S. Gray, P. A. Cohen, Y. Yu and A. R. R. Forrest, *Nat. Commun.*, 2024, **15**, 2860.
34 A. Garrido-Trigo, A. M. Corraliza, M. Veny, I. Dotti, E. Melón-Ardanaz, A. Rill, H. L. Crowell, Á. Corbí, V. Gudiño, M. Esteller, I. Álvarez-Teubel, D. Aguilar, M. C. Masamunt, E. Killingbeck, Y. Kim, M. Leon, S. Visvanathan, D. Marchese, G. Caratù, A. Martin-Cardona, M. Esteve, I. Ordás, J. Panés, E. Ricart, E. Mereu, H. Heyn and A. Salas, *Nat. Commun.*, 2023, **14**, 4506.
35 S. He, R. Bhatt, C. Brown, E. A. Brown, D. L. Buhr, K. Chantranuvatana, P. Danaher, D. Dunaway, R. G. Garrison, G. Geiss, M. T. Gregory, M. L. Hoang, R. Khafizov, E. E. Killingbeck, D. Kim, T. K. Kim, Y. Kim, A. Klock, M. Korukonda, A. Kutchma, Z. R. Lewis, Y. Liang, J. S. Nelson, G. T. Ong, E. P. Perillo, J. C. Phan, T. Phan-Everson, E. Piazza, T. Rane, Z. Reitz, M. Rhodes, A. Rosenbloom, D. Ross, H. Sato, A. W. Wardhani, C. A. Williams-Wietzikoski, L. Wu and J. M. Beechem, *Nat. Biotechnol.*, 2022, **40**, 1794–1806.
36 R. Ke, M. Mignardi, A. Pacureanu, J. Svedlund, J. Botling, C. Wählby and M. Nilsson, *Nat. Methods*, 2013, **10**, 857–860.
37 D. Gyllborg, C. M. Langseth, X. Qian, E. Choi, S. M. Salas, M. M. Hilscher, E. S. Lein and M. Nilsson, *Nucleic Acids Res.*, 2020, **48**, e112.
38 X. Wang, W. E. Allen, M. A. Wright, E. L. Sylwestrak, N. Samusik, S. Vesuna, K. Evans, C. Liu, C. Ramakrishnan, J. Liu, G. P. Nolan, F. A. Bava and K. Deisseroth, *Science*, 2018, **361**, eaat5691.
39 S. Liu, S. Punthambaker, E. P. R. Iyer, T. Ferrante, D. Goodwin, D. Fürth, A. C. Pawlowski, K. Jindal, J. M. Tam, L. Mifflin, S. Alon, A. Sinha, A. T. Wassie, F. Chen, A. Cheng, V. Willocq, K. Meyer, K. H. Ling, C. K. Camplisson, R. E. Kohman, J. Aach, J. H. Lee, B. A. Yankner, E. S. Boyden and G. M. Church, *Nucleic Acids Res.*, 2021, **49**, e58.
40 J. Ren, H. Zhou, H. Zeng, C. K. Wang, J. Huang, X. Qiu, X. Sui, Q. Li, X. Wu, Z. Lin, J. A. Lo, K. Maher, Y. He, X. Tang, J. Lam, H. Chen, B. Li, D. E. Fisher, J. Liu and X. Wang, *Nat. Methods*, 2023, **20**, 695–705.
41 J. H. Lee, E. R. Daugharthy, J. Scheiman, R. Kalhor, T. C. Ferrante, J. L. Yang, R. Terry, S. F. Jeanty, C. Li, R. Amamoto, D. T. Peters, B. M. Turczyk, A. H. Marblestone, S. A. Inverso, A. Bernard, P. Mali, X. Rios, J. Aach and G. M. Church, *Science*, 2014, **343**, 1360–1363.
42 J. H. Lee, E. R. Daugharthy, J. Scheiman, R. Kalhor, T. C. Ferrante, R. Terry, B. M. Turczyk, J. L. Yang, H. S. Lee, J. Aach, K. Zhang and G. M. Church, *Nat. Protoc.*, 2015, **10**, 442–458.

43 S. Alon, D. R. Goodwin, A. Sinha, A. T. Wassie, F. Chen, E. R. Daugharthy, Y. Bando, A. Kajita, A. G. Xue, K. Marrett, R. Prior, Y. Cui, A. C. Payne, C. C. Yao, H.-J. Suk, R. Wang, C.-C. (Jay) Yu, P. Tillberg, P. Reginato, N. Pak, S. Liu, S. Punthambaker, E. P. R. Iyer, R. E. Kohman, J. A. Miller, E. S. Lein, A. Lako, N. Cullen, S. Rodig, K. Helvie, D. L. Abravanel, N. Wagle, B. E. Johnson, J. Klughammer, M. Slyper, J. Waldman, J. Jané-Valbuena, O. Rozenblatt-Rosen, A. Regev, I. Consortium, G. M. Church, A. H. Marblestone and E. S. Boyden, *Science*, 2021, **371**, eaax2656.
44 H. Q. Nguyen, S. Chattoraj, D. Castillo, S. C. Nguyen, G. Nir, A. Lioutas, E. A. Hershberg, N. M. C. Martins, P. L. Reginato, M. Hannan, B. J. Beliveau, G. M. Church, E. R. Daugharthy, M. A. Marti-Renom and C. Ting Wu, *Nat. Methods*, 2020, **17**, 822–832.
45 B. J. Beliveau, A. N. Boettiger, M. S. Avendaño, R. Jungmann, R. B. McCole, E. F. Joyce, C. Kim-Kiselak, F. Bantignies, C. Y. Fonseka, J. Erceg, M. A. Hannan, H. G. Hoang, D. Colognori, J. T. Lee, W. M. Shih, P. Yin, X. Zhuang and C. Wu, *Nat. Commun.*, 2015, **6**, 7147.
46 T. Lohoff, S. Ghazanfar, A. Missarova, N. Koulena, N. Pierson, J. A. Griffiths, E. S. Bardot, C.-H. L. Eng, R. C. V. Tyser, R. Argelaguet, C. Guibentif, S. Srinivas, J. Briscoe, B. D. Simons, A.-K. Hadjantonakis, B. Göttgens, W. Reik, J. Nichols, L. Cai and J. C. Marioni, *Nat. Biotechnol.*, 2022, **40**, 74–85.
47 Y. Fan, Ž. Andrusivová, Y. Wu, C. Chai, L. Larsson, M. He, L. Luo, J. Lundeberg and B. Wang, *Nat. Methods*, 2023, **20**, 1179–1182.
48 S. G. Rodriques, R. R. Stickels, A. Goeva, C. A. Martin, E. Murray, C. R. Vanderburg, J. Welch, L. M. Chen, F. Chen and E. Z. Macosko, *Science*, 2019, **363**, 1463–1467.
49 R. R. Stickels, E. Murray, P. Kumar, J. Li, J. L. Marshall, D. J. Di Bella, P. Arlotta, E. Z. Macosko and F. Chen, *Nat. Biotechnol.*, 2021, **39**, 313–319.
50 C.-S. Cho, J. Xi, Y. Si, S.-R. Park, J.-E. Hsu, M. Kim, G. Jun, H. M. Kang and J. H. Lee, *Cell*, 2021, **184**, 3559–3572.e22.
51 A. Chen, S. Liao, M. Cheng, K. Ma, L. Wu, Y. Lai, X. Qiu, J. Yang, J. Xu, S. Hao, X. Wang, H. Lu, X. Chen, X. Liu, X. Huang, Z. Li, Y. Hong, Y. Jiang, J. Peng, S. Liu, M. Shen, C. Liu, Q. Li, Y. Yuan, X. Wei, H. Zheng, W. Feng, Z. Wang, Y. Liu, Z. Wang, Y. Yang, H. Xiang, L. Han, B. Qin, P. Guo, G. Lai, P. Muñoz-Cánoves, P. H. Maxwell, J. P. Thiery, Q.-F. Wu, F. Zhao, B. Chen, M. Li, X. Dai, S. Wang, H. Kuang, J. Hui, L. Wang, J.-F. Fei, O. Wang, X. Wei, H. Lu, B. Wang, S. Liu, Y. Gu, M. Ni, W. Zhang, F. Mu, Y. Yin, H. Yang, M. Lisby, R. J. Cornall, J. Mulder, M. Uhlén, M. A. Esteban, Y. Li, L. Liu, X. Xu and J. Wang, *Cell*, 2022, **185**, 1777–1792.e21.
52 R. Drmanac, A. B. Sparks, M. J. Callow, A. L. Halpern, N. L. Burns, B. G. Kermani, P. Carnevali, I. Nazarenko, G. B. Nilsen, G. Yeung, F. Dahl, A. Fernandez, B. Staker, K. P. Pant, J. Baccash, A. P. Borcherding, A. Brownley, R. Cedeno, L. Chen, D. Chernikoff, A. Cheung, R. Chirita, B. Curson, J. C. Ebert, C. R. Hacker, R. Hartlage, B. Hauser, S. Huang, Y. Jiang, V. Karpinchyk, M. Koenig, C. Kong, T. Landers, C. Le, J. Liu, C. E. McBride, M. Morenzoni, R. E. Morey, K. Mutch, H. Perazich, K. Perry, B. A. Peters, J. Peterson, C. L. Pethiyagoda, K. Pothuraju, C. Richter, A. M. Rosenbaum, S. Roy, J. Shafto, U. Sharanhovich, K. W. Shannon, C. G. Sheppy, M. Sun, J. V. Thakuria, A. Tran, D. Vu, A. W. Zaranek, X. Wu, S. Drmanac, A. R. Oliphant, W. C. Banyai, B. Martin, D. G. Ballinger, G. M. Church and C. A. Reid, *Science*, 2010, **327**, 78–81.
53 J. Du, Y. Yang, Z. An, M. Zhang, X. Fu, Z. Huang, Y. Yuan and J. Hou, *J. Transl. Med.*, 2023, **21**, 330.
54 H. Xu, H. Fu, Y. Long, K. Ang, R. Sethi, K. Chong, M. Li, R. Uddamvathanak, H. Lee, J. Ling, A. Chen, L. Shao, L. Liu and J. Chen, *Genome Med.*, 2024, **16**, 12.
55 Y. Chen, J. Liu, Y. Jiang, A. Ma, Y. Yeo, Q. Guo, M. McNutt, J. E. Krull, S. J. Rodig, D. H. Barouch, G. P. Nolan, D. Xu, S. Jiang, Z. Li, B. Liu and Q. Ma, *Nat. Commun.*, 2024, **15**, 7467.
56 L. Moses and L. Pachter, *Nat. Methods*, 2022, **19**, 534–546.
57 L. Liu, A. Chen, Y. Li, J. Mulder, H. Heyn and X. Xu, *Cell*, 2024, **187**, 4488–4519.
58 Y. You, Y. Fu, L. Li, Z. Zhang, S. Jia, S. Lu, W. Ren, Y. Liu, Y. Xu, X. Liu, F. Jiang, G. Peng, A. S. Kumar, M. E. Ritchie, X. Liu and L. Tian, *Nat. Methods*, 2024, **21**, 1743–1754.
59 L. C. Gaspard-Boulinc, L. Gortana, T. Walter, E. Barillot and F. M. G. Cavalli, *Nat. Rev. Genet.*, 2025, DOI: **10.1038/s41576-025-00845-y**.
60 K. J. Westerich, K. S. Chandrasekaran, T. Gross-Thebing, N. Kueck, E. Raz and A. Rentmeister, *Chem. Sci.*, 2020, **11**, 3089–3095.
61 S. Tyagi and F. R. Kramer, *Nat. Biotechnol.*, 1996, **14**, 303–308.
62 X. H. Peng, Z. H. Cao, J. T. Xia, G. W. Carlson, M. M. Lewis, W. C. Wood and L. Yang, *Cancer Res.*, 2005, **65**, 1909–1917.
63 C. D. Medley, T. J. Drake, J. M. Tomasini, R. J. Rogers and W. Tan, *Anal. Chem.*, 2005, **77**, 4713–4718.
64 W. Pan, T. Zhang, H. Yang, W. Diao, N. Li and B. Tang, *Anal. Chem.*, 2013, **85**, 10581–10588.
65 A. S. Walsh, H. Yin, C. M. Erben, M. J. A. Wood and A. J. Turberfield, *ACS Nano*, 2011, **5**, 5427–5432.
66 L. Liang, J. Li, Q. Li, Q. Huang, J. Shi, H. Yan and C. Fan, *Angew. Chem., Int. Ed.*, 2014, **53**, 7745–7750.
67 J. Li, H. Pei, B. Zhu, L. Liang, M. Wei, Y. He, N. Chen, D. Li, Q. Huang and C. Fan, *ACS Nano*, 2011, **5**, 8783–8789.
68 W. Zhou, D. Li, C. Xiong, R. Yuan and Y. Xiang, *ACS Appl. Mater. Interfaces*, 2016, **8**, 13303–13308.
69 Z. Zhou, Y. S. Sohn, R. Nechushtai and I. Willner, *ACS Nano*, 2020, **14**, 9021–9031.
70 S. Wang, M. Xia, J. Liu, S. Zhang and X. Zhang, *ACS Sens.*, 2017, **2**, 735–739.
71 F. Yang, Y. Cheng, Y. Zhang, W. Wei, H. Dong, H. Lu and X. Zhang, *Anal. Chem.*, 2020, **92**, 4411–4418.
72 E. Benson, A. Mohammed, J. Gardell, S. Masich, E. Czeizler, P. Orponen and B. Högberg, *Nature*, 2015, **523**, 441–444.

73 S. Dey, C. Fan, K. V. Gothelf, J. Li, C. Lin, L. Liu, N. Liu, M. A. D. Nijenhuis, B. Saccà, F. C. Simmel, H. Yan and P. Zhan, *Nat. Rev. Methods Primers*, 2021, **1**, 13.
74 S. Karkare and D. Bhatnagar, *Appl. Microbiol. Biotechnol.*, 2006, **71**, 575–586.
75 M. Mondal, R. Liao, C. D. Nazaroff, A. D. Samuel and J. Guo, *Chem. Sci.*, 2018, **9**, 2909–2917.
76 Z. Qing, J. Xu, J. Hu, J. Zheng, L. He, Z. Zou, S. Yang, W. Tan and R. Yang, *Angew. Chem., Int. Ed.*, 2019, **58**, 11574–11585.
77 H. M. T. Choi, J. Y. Chang, L. A. Trinh, J. E. Padilla, S. E. Fraser and N. A. Pierce, *Nat. Biotechnol.*, 2010, **28**, 1208–1212.
78 J. Hemphill and A. Deiters, *J. Am. Chem. Soc.*, 2013, **135**, 10512–10518.
79 H. Wu, B. T. Cisneros, C. M. Cole and N. K. Devaraj, *J. Am. Chem. Soc.*, 2014, **136**, 17942–17945.
80 H. Wu, S. C. Alexander, S. Jin and N. K. Devaraj, *J. Am. Chem. Soc.*, 2016, **138**, 11429–11432.
81 Y. Deng, T. Shen, X. Yu, J. Li, P. Zou, Q. Gong, Y. Zheng, H. Sun, X. Liu and H. Wu, *Angew. Chem., Int. Ed.*, 2024, **63**, e202319853.
82 A. Yu, X. He, T. Shen, X. Yu, W. Mao, W. Chi, X. Liu and H. Wu, *Chem. Soc. Rev.*, 2025, **54**, 2984–3016.
83 S.-J. Zhao, P. Zheng, Z. Wu and J.-H. Jiang, *Anal. Chem.*, 2022, **94**, 2693–2698.
84 Z. He, S. Peng, Q. Wei, S. Jia, S. Guo, K. Chen and X. Zhou, *CCS Chem.*, 2020, **2**, 89–97.
85 J. Ge, J. Han, X. Fang, C. Wang and Y. Yang, *ACS Chem. Biol.*, 2025, **20**, 1884–1891.
86 D. Ganz, D. Harijan and H.-A. Wagenknecht, *RSC Chem. Biol.*, 2020, **1**, 86–97.
87 W. Pan, B. Liu, X. Gao, Z. Yu, X. Liu, N. Li and B. Tang, *Nanoscale*, 2018, **10**, 14264–14271.
88 H. Jiang, F. R. Li, W. Li, X. Lu and K. Ling, *Microchim. Acta*, 2018, **185**, 552.
89 A. E. Prigodich, P. S. Randeria, W. E. Briley, N. J. Kim, W. L. Daniel, D. A. Giljohann and C. A. Mirkin, *Anal. Chem.*, 2012, **84**, 2062–2066.
90 L.-S. Lin, Z.-X. Cong, J.-B. Cao, K.-M. Ke, Q.-L. Peng, J. Gao, H.-H. Yang, G. Liu and X. Chen, *ACS Nano*, 2014, **8**, 3876–3883.
91 S. Lange, Y. Katayama, M. Schmid, O. Burkacky, C. Bräuchle, D. C. Lamb and R. Jansen, *Traffic*, 2008, **9**, 1256–1267.
92 S. Hocine, P. Raymond, D. Zenklusen, J. A. Chao and R. H. Singer, *Nat. Methods*, 2013, **10**, 119–121.
93 T. Fukaya, B. Lim and M. Levine, *Cell*, 2016, **166**, 358–368.
94 B. Lim, T. Fukaya, T. Heist and M. Levine, *Proc. Natl. Acad. Sci. U. S. A.*, 2018, **115**, 8376–8381.
95 E. Tutucci, M. Vera, J. Biswas, J. Garcia, R. Parker and R. H. Singer, *Nat. Methods*, 2018, **15**, 81–89.
96 N. Katz, E. Tripto, N. Granik, S. Goldberg, O. Atar, Z. Yakhini, Y. Orenstein and R. Amit, *Nat. Commun.*, 2021, **12**, 1576.
97 H. Manghwar, K. Lindsey, X. Zhang and S. Jin, *Trends Plant Sci.*, 2019, **24**, 1102–1125.
98 J. Y. Wang and J. A. Doudna, *Science*, 2023, **379**, eadd8643.
99 E. Park and H. Kim, *Exp. Mol. Med.*, 2025, **57**, 1392–1399.
100 X. Xu and L. S. Qi, *J. Mol. Biol.*, 2019, **431**, 34–47.
101 H. Wang, M. Nakamura, T. R. Abbott, D. Zhao, K. Luo, C. Yu, C. M. Nguyen, A. Lo, T. P. Daley, M. La Russa, Y. Liu and L. S. Qi, *Science*, 2019, **365**, 1301–1305.
102 L. Z. Yang, Y. Wang, S. Q. Li, R. W. Yao, P. F. Luan, H. Wu, G. G. Carmichael and L. L. Chen, *Mol. Cell*, 2019, **76**, 981–997.e7.
103 L. Z. Yang, B. Q. Gao, Y. Huang, Y. Wang, L. Yang and L. L. Chen, *Cell Insight*, 2022, **1**, 100044.
104 H. Ma, L. C. Tu, A. Naseri, M. Huisman, S. Zhang, D. Grunwald and T. Pederson, *Nat. Biotechnol.*, 2016, **34**, 528–530.
105 H. Tang, J. Peng, S. Peng, Q. Wang, X. Jiang, X. Xue, Y. Tao, L. Xiang, Q. Ji, S.-M. Liu, X. Weng and X. Zhou, *Chem. Sci.*, 2022, **13**, 14032–14040.
106 G. Zhu, X. Zhou, M. Wen, J. Qiao, G. Li and Y. Yao, *BioDesign Res.*, 2024, **6**, 0041.
107 D. A. Nelles, M. Y. Fang, M. R. O'Connell, J. L. Xu, S. J. Markmiller, J. A. Doudna and G. W. Yeo, *Cell*, 2016, **165**, 488–496.
108 Z. Fan, F. Liu, F. Wang, X. Chu, J. Jiang, *Research Square*, DOI: **10.21203/rs.3.rs-1435078/v1**.
109 H. Y. Jia, X. Y. Zhang, B. C. Ye and B. C. Yin, *Anal. Chem.*, 2024, **96**, 5913–5921.
110 D. Colognori, M. Trinidad and J. A. Doudna, *Nat. Biotechnol.*, 2023, **41**, 1256–1264.
111 C. Xia, D. Colognori, X. S. Jiang, K. Xu and J. A. Doudna, *Nat. Biotechnol.*, 2025, DOI: **10.1038/s41587-024-02540-5**.
112 X. Lu, K. Y. S. Kong and P. J. Unrau, *Chem. Soc. Rev.*, 2023, **52**, 4071–4098.
113 J. S. Paige, K. Y. Wu and S. R. Jaffrey, *Science*, 2011, **333**, 642–646.
114 A. P. K. K. Karunanayake Mudiyanselage, R. Wu, M. A. Leon-Duque, K. Ren and M. You, *Methods*, 2019, **161**, 24–34.
115 Y. Su and M. C. Hammond, *Curr. Opin. Biotechnol.*, 2020, **63**, 157–166.
116 Q. Yu, K. Ren and M. You, *Nanoscale*, 2021, **13**, 7988–8003.
117 J. Wu, N. Svensen, W. Song, H. Kim, S. Zhang, X. Li and S. R. Jaffrey, *J. Am. Chem. Soc.*, 2022, **144**, 5471–5477.
118 S. K. Dey, G. S. Filonov, A. O. Olarerin-George, B. T. Jackson, L. W. S. Finley and S. R. Jaffrey, *Nat. Chem. Biol.*, 2022, **18**, 180–190.
119 A. Arora, M. Sunbul and A. Jäschke, *Nucleic Acids Res.*, 2015, **43**, gkv718.
120 M. D. E. Jepsen, S. M. Sparvath, T. B. Nielsen, A. H. Langvad, G. Grossi, K. V. Gothelf and E. S. Andersen, *Nat. Commun.*, 2018, **9**, 18.
121 R. Wu, A. P. K. K. Karunanayake Mudiyanselage, F. Shafiei, B. Zhao, Y. Bagheri, Q. Yu, K. McAuliffe, K. Ren and M. You, *Angew. Chem., Int. Ed.*, 2019, **58**, 18271–18275.
122 R. Wu, A. P. K. K. Karunanayake Mudiyanselage, K. Ren, Z. Sun, Q. Tian, B. Zhao, Y. Bagheri, D. Lutati, P. Keshri and M. You, *ACS Appl. Bio Mater.*, 2020, **3**, 2633–2642.
123 P. Yin, M. Ge, S. Xie, L. Zhang, S. Kuang and Z. Nie, *Chem. Sci.*, 2023, **14**, 14131–14139.

124 L. Jiang, X. Xie, N. Su, D. Zhang, X. Chen, X. Xu, B. Zhang, K. Huang, J. Yu, M. Fang, B. Bao, F. Zuo, L. Yang, R. Zhang, H. Li, X. Huang, Z. Chen, Q. Zeng, R. Liu, Q. Lin, Y. Zhao, A. Ren, L. Zhu and Y. Yang, *Nat. Methods*, 2023, **20**, 1563–1572.
125 P. Yin, C. Huang, L. Zhang, Z. Li, C. Zhong, S. Kuang, C. Lei, Y. Huang and Z. Nie, *Angew. Chem., Int. Ed.*, 2025, **64**, e202424060.
126 L. Jiang, F. Zuo, Y. Pan, R. Li, Y. Shi, X. Huang, D. Zhang, Y. Zhuang, Y. Zhao, Q. Lin, Y. Yang, L. Zhu and X. Chen, *Small*, 2025, **21**, 2405165.
127 R. Zheng, R. Wu, Y. Liu, Z. Sun, Z. Xue, Y. Bagheri, S. Khajouei, L. Mi, Q. Tian, R. Pho, Q. Liu, S. Siddiqui, K. Ren and M. You, *Nucleic Acids Res.*, 2024, **52**, e67.
128 E. Braselmann, A. J. Wierzba, J. T. Polaski, M. Chromiński, Z. E. Holmes, S.-T. Hung, D. Batan, J. R. Wheeler, R. Parker, R. Jimenez, D. Gryko, R. T. Batey and A. E. Palmer, *Nat. Chem. Biol.*, 2018, **14**, 964–971.
129 N. Sarfraz, E. Moscoso, T. Oertel, H. J. Lee, S. Ranjit and E. Braselmann, *Nat. Commun.*, 2023, **14**, 867.
130 J. Wu, S. Zaccara, D. Khuperkar, H. Kim, M. E. Tanenbaum and S. R. Jaffrey, *Nat. Methods*, 2019, **16**, 862–865.
131 T. G. Pham, O. Ajayi and J. Wu, *bioRxiv*, 2024, DOI: **10.1101/2024.12.16.628815**.
132 C. J. Kuffner, A. M. Marzilli and J. T. Ngo, *bioRxiv*, 2024, DOI: **10.1101/2024.11.21.624393**.
133 W. Zhou, M. Wu, X. Shao, L. Tang, F. Wang and J. Jiang, *Angew. Chem., Int. Ed.*, 2025, e202502350.
134 J.-H. Su, P. Zheng, S. S. Kinrot, B. Bintu and X. Zhuang, *Cell*, 2020, **182**, 1641–1659.e26.
135 D. Feldman, A. Singh, J. L. Schmid-Burgk, R. J. Carlson, A. Mezger, A. J. Garrity, F. Zhang and P. C. Blainey, *Cell*, 2019, **179**, 787–799.e17.
136 A. Coulon, M. L. Ferguson, V. De Turris, M. Palangat, C. C. Chow and D. R. Larson, *eLife*, 2014, **3**, e03939.
137 Z. Waks, A. M. Klein and P. A. Silver, *Mol. Syst. Biol.*, 2011, **7**, 506.
138 J. M. Halstead, T. Lionnet, J. H. Wilbertz, F. Wippich, A. Ephrussi, R. H. Singer and J. A. Chao, *Science*, 2015, **347**, 1367–1671.
139 I. Horvathova, F. Voigt, A. V. Kotrys, Y. Zhan, C. G. Artus-Revel, J. Eglinger, M. B. Stadler, L. Giorgetti and J. A. Chao, *Mol. Cell*, 2017, **68**, 615–625.e9.
140 J. H. Wilbertz, F. Voigt, I. Horvathova, G. Roth, Y. Zhan and J. A. Chao, *Mol. Cell*, 2019, **73**, 946–958.e7.
141 A. E. Moor, M. Golan, E. E. Massasa, D. Lemze, T. Weizman, R. Shenhav, S. Baydatch, O. Mizrahi, R. Winkler, O. Golani, N. Stern-Ginossar and S. Itzkovitz, *Science*, 2017, **357**, 1299–1303.
142 V. Gandin, J. Kim, L.-Z. Yang, Y. Lian, T. Kawase, A. Hu, K. Rokicki, G. Fleishman, P. Tillberg, A. A. Castrejon, C. Stringer, S. Preibisch and Z. J. Liu, *Science*, 2025, **388**, eadq2084.
143 G. M. Wadsworth, S. Srinivasan, L. B. Lai, M. Datta, V. Gopalan and P. R. Banerjee, *Mol. Cell*, 2024, **84**, 3692–3705.
144 E. Tutucci, N. M. Livingston, R. H. Singer and B. Wu, *Annu. Rev. Biophys.*, 2018, **47**, 85–106.
145 T. Matheny, B. S. Rao and R. Parker, *Mol. Cell. Biol.*, 2019, **39**, e00313–e00319.
146 C. L. Riggs, N. Kedersha, P. Ivanov and P. Anderson, *J. Cell Sci.*, 2020, **133**, jcs242487.
147 Z. Xue, K. Ren, R. Wu, Z. Sun, R. Zheng, Q. Tian, A. A. Ali, L. Mi and M. You, *Nucleic Acids Res.*, 2023, **51**, 8337–8347.
148 A. Fortner and O. Bucur, *Front. Cell Dev. Biol.*, 2024, **12**, 1378875.
149 J. Ren, S. Luo, H. Shi and X. Wang, *Mol. Cell*, 2024, **84**, 3737–3757.
150 L. Tian, F. Chen and E. Z. Macosko, *Nat. Biotechnol.*, 2023, **41**, 773–782.
151 C. G. Williams, H. J. Lee, T. Asatsuma, R. Vento-Tormo and A. Haque, *Genome Med.*, 2022, **14**, 68.
152 B. Turner-Bridger, C. Caterino and J.-M. Cioni, *Open Biol.*, 2020, **10**, 200177.
153 H. Yoshimura, *Biochemistry*, 2018, **57**, 200–208.
154 H. Yoshimura, A. Inaguma, T. Yamada and T. Ozawa, *ACS Chem. Biol.*, 2012, **7**, 999–1005.
155 J. Tilsner, O. Linnik, N. M. Christensen, K. Bell, I. M. Roberts, C. Lacomme and K. J. Oparka, *Plant J.*, 2009, **57**, 758–770.
156 A. P. K. K. Karunanayake Mudiyanselage, Q. Yu, M. A. Leon-Duque, B. Zhao, R. Wu and M. You, *J. Am. Chem. Soc.*, 2018, **140**, 8739–8745.
157 K. Ren, R. Wu, A. P. K. K. Karunanayake Mudiyanselage, Q. Yu, B. Zhao, Y. Xie, Y. Bagheri, Q. Tian and M. You, *J. Am. Chem. Soc.*, 2020, **142**, 2968–2974.
158 K. C. Jackson and L. Pachter, *Cell Genomics*, 2023, **3**, 100374.
159 R. Horton and A. Lucassen, *N. Bioeth.*, 2023, **29**, 37–51.
160 S. Sawaya, C. Lo, P. Li, B. Hovde and P. Chain, *medRxiv*, 2024, DOI: **10.1101/2024.11.29.24318203**.